NATIONAL ADVISORY COMMITTEE FOR AERONAUTICS
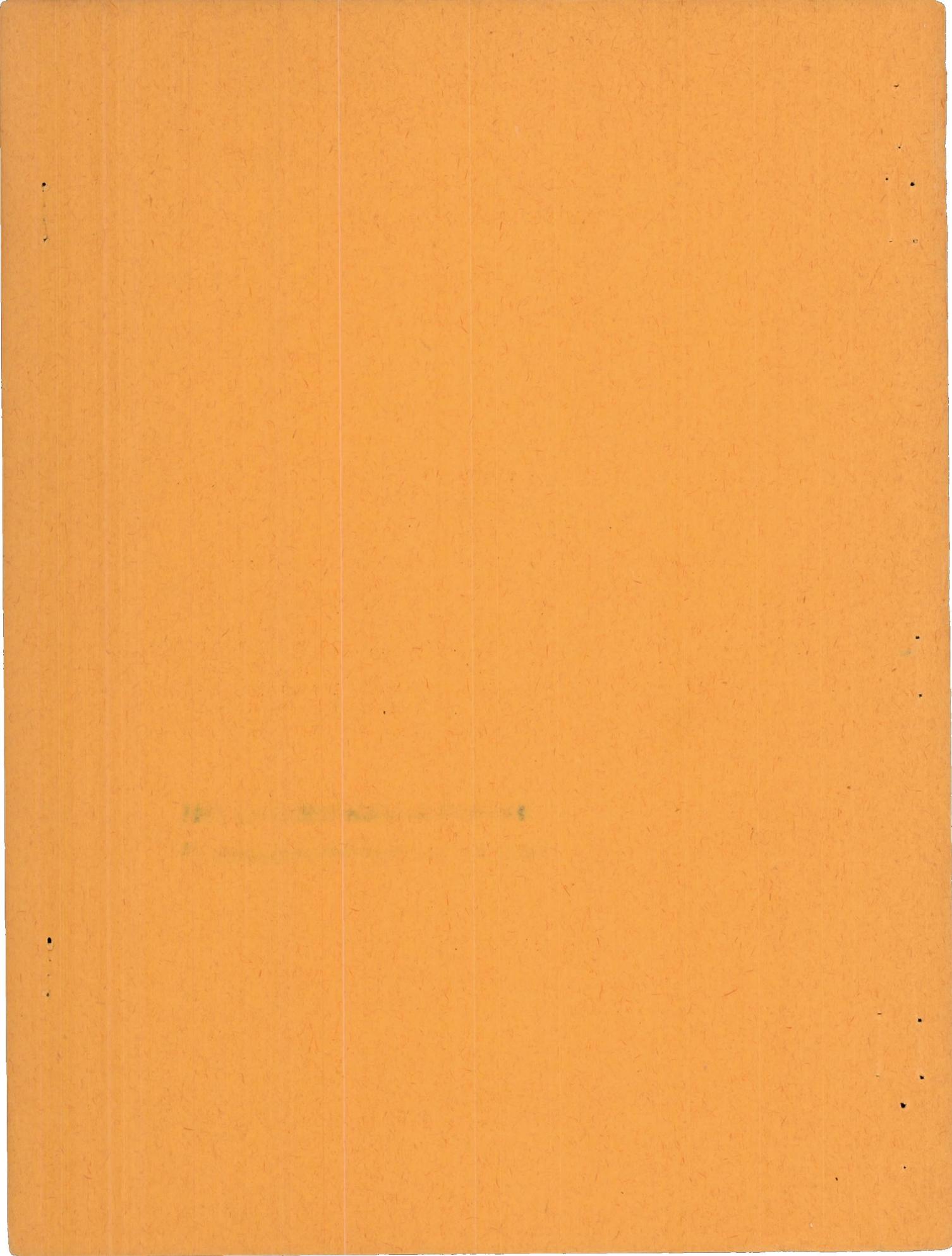
TECHNICAL NOTE

No. 1048

TWO-DIMENSIONAL WIND-TUNNEL INVESTIGATION OF LOW-DRAG

VERTICAL-TAIL, HORIZONTAL-TAIL, AND WING

SECTIONS EQUIPPED WITH SEALED INTERNALLY

BALANCED CONTROL SURFACES

By Albert L. Braslow

Langley Memorial Aeronautical Laboratory
Langley Field, Va.

Washington
April 1946

NATIONAL ADVISORY COMMITTEE FOR AERONAUTICS

TECHNICAL NOTE NO. 1048

TWO-DIMENSIONAL WIND-TUNNEL INVESTIGATION OF LOW-DRAG

VERTICAL-TAIL, HORIZONTAL-TAIL, AND WING

SECTIONS EQUIPPED WITH SEALED INTERNALLY

BALANCED CONTROL SURFACES

By Albert L. Braslow

SUMMARY

A two-dimensional wind-tunnel investigation was
made of three low-drag airfoil sections equipped with
sealed internally balanced control surfaces designed
for use as vertical-tail, horizontal-tail, and wing
sections. The tests included determination of control-
surface effectiveness and hinge moments and airfoil
section drag characteristics. Balance pressures were
also measured for use in estimating the hinge-moment
characteristics of the control surfaces with any amount
of sealed internal balance.

Sharp irregularities occurred in the variation of
the control-surface section hinge-moment coefficient
with airfoil section angle of attack, which were probably
caused by sudden movements in transition along the sur-
faces of all three airfoils at the extremities of the
low-drag range. Tests of the vertical-tail section
indicated that these irregularities were reduced in
magnitude when transition was fixed at a forward chord-
wise position but were not entirely removed until transi-
tion was fixed at the airfoil leading edge. An estimated
variation of aileron wheel force with wing-tip helix
angle for an assumed airplane indicated that no unusual
aileron wheel-force characteristics would be caused by
the irregularities in the two-dimensional hinge-moment
characteristics. Sudden movements in transition along
the surfaces of vertical-tail or horizontal-tail sections,
however, would probably cause sudden changes in rudder or
elevator hinge moments.

INTRODUCTION

The recent trend toward the use of large high-speed airplanes has imposed upon the airplane designer the problem of obtaining adequate control effectiveness without excessive control forces while securing low values of airfoil drag and high values of critical Mach number. Data for use by the designer in the prediction of low-drag-wing characteristics are available but only a limited amount of data on two-dimensional aerodynamic characteristics of control surfaces on low-drag airfoils is available. An investigation was made in the Langley two-dimensional low-turbulence pressure tunnel of two NACA 64-series-type airfoils and one NACA 7-series-type airfoil equipped with sealed internally balanced control surfaces to provide additional data on two-dimensional characteristics of control surfaces on low-drag airfoils. The 64-series-type airfoils were intended for use as tail surfaces and were equipped with a rudder and elevator of 0.40 and 0.35 airfoil chord, respectively. The 7-series-type airfoil was fitted with an aileron of 0.22 airfoil chord.

The tests, which were made at Reynolds numbers of 3×10^6, 6×10^6, and 9×10^6, included the determination of control-surface effectiveness and hinge moments and airfoil section drag characteristics. The pressure differences across the control-surface seals were also obtained for use in estimating the hinge-moment characteristics of the control surfaces with any amount of sealed internal balance.

SYMBOLS AND COEFFICIENTS

The symbols and coefficients used in the presentation of results are defined as follows:

a_o airfoil section angle of attack, degrees

c chord of airfoil with control surface neutral; measured along maximum length line

c_x chord of control surface measured from hinge axis to trailing edge

c_b chord of overhang from control-surface hinge axis to middle of gap seal

δ_x control-surface deflection with respect to airfoil; positive when trailing edge is deflected downward

R Reynolds number

q_o free-stream dynamic pressure

b total wing span

b_a span of one aileron

$\bar{c}_a$ root-mean-square chord of aileron behind hinge axis

V true airspeed

V_i indicated airspeed

p local static pressure; also, rolling velocity when used in parameter $pb/2V$

H_o free-stream total pressure

S airfoil pressure coefficient $\dfrac{H_o - p}{q_o}$

$pb/2V$ helix angle described by wing tip during roll, radians

F_w wheel force

θ wheel deflection from neutral

C_{l_δ} rate of change of rolling-moment coefficient with aileron deflection

C_{l_p} rate of change of rolling-moment coefficient with $pb/2V$

c_l airfoil section lift coefficient

Δc_l increment of c_l caused by deflection of control surface from neutral

c_d airfoil section drag coefficient

h control-surface hinge moment per unit span;
positive when control surface tends to
deflect downward

c_{h_x} control-surface section hinge-moment coefficient
based on control-surface chord $\left(\dfrac{h}{q_o c_x^2}\right)$

$\left(c_{h_a}\right)_{up}$ hinge-moment coefficient of upgoing aileron
estimated for airplane during roll

$\left(c_{h_a}\right)_{down}$ hinge-moment coefficient of downgoing aileron
estimated for airplane during roll

$\Delta p / q_o$ seal-pressure-difference coefficient (ratio
of pressure difference across control-
surface seal to free-stream dynamic
pressure); positive when pressure below
seal is greater than pressure above seal

$\left(\dfrac{\partial c_l}{\partial \alpha_o}\right)_{\delta_x}$ rate of change of section lift coefficient
with section angle of attack

$\left(\dfrac{\partial c_l}{\partial \delta_x}\right)_{\alpha_o}$ rate of change of section lift coefficient
with control-surface deflection

$\left(\dfrac{\partial \alpha_o}{\partial \delta_x}\right)_{c_l}$ control-surface section effectiveness parameter
(absolute value); also designated as k for
aileron

$\left(\dfrac{\Delta \alpha_o}{\Delta \delta_a}\right)_{c_l}$ aileron section effectiveness parameter
(ratio of increment of airfoil section
angle of attack to increment of aileron
deflection required to maintain a constant
lift coefficient; absolute value)

$\left(\dfrac{\partial c_{h_x}}{\partial \alpha_o}\right)_{\delta_x}$ rate of change of section hinge-moment
coefficient with section angle of attack

$\left(\dfrac{\partial c_{h_x}}{\partial \delta_x}\right)_{\alpha_o}$ rate of change of section hinge-moment coeffi-
cient with control-surface deflection

The subscript x is replaced herein with subscripts r, e, and a for the rudder, elevator, and aileron, respectively. The subscripts to the partial derivatives denote the variables held constant when the partial derivatives are taken. The derivatives are obtained at zero angle of attack and zero control-surface deflection except as noted.

MODELS AND APPARATUS

The three models, having chords of 24 inches, were two-dimensional airfoil sections designed for use as a vertical tail, a horizontal tail, and a wing and were constructed of laminated mahogany. Sketches of the models are presented as figure 1. Rubber seals were used along the complete span and at both ends of the control surfaces to prevent the flow of air through the gaps.

The pressure difference across the control-surface seals was measured with static-pressure orifices located above and below the balance plates. A manometer setup, which integrated the pressures along the floor and ceiling of the tunnel test section, was used to measure lift, and the wake survey method was used to measure drag. Hinge moments of the control surfaces were measured with electrical-resistance strain gages.

The vertical-tail section was a 0.155c thick symmetrical airfoil with a pressure distribution (fig. 2) similar to that of the NACA 64-series airfoils. The model was equipped with a 0.40c rudder with a sealed internal balance of 0.412c_r, that is, $\dfrac{c_b}{c_r} = 0.412$.

The horizontal-tail section, which also had a pressure distribution (fig. 3) similar to that of the NACA 64-series airfoils, had a maximum thickness of approximately 0.13c. The angle of attack for this model was measured with respect to a reference line shown in figure 1. The model was equipped with a 0.35c elevator with a sealed internal balance of approximately 0.43c_e.

The wing profile had a maximum thickness of approximately 0.17c and a pressure distribution (fig. 4) similar to that of an NACA 7-series airfoil. The design section lift coefficient is 0.266, for which the position of

minimum pressure is approximately 0.35c on the upper
surface and 0.50c on the lower surface. The airfoil
section angle of attack was measured with respect to a
reference line shown in figure 1. The model was equipped
with a 0.22c aileron of true airfoil contour with a sealed
internal balance of approximately $0.44c_a$.

For the normal smooth condition of the models, the
airfoil surfaces were sanded with No. 400 carborundum
paper to produce an aerodynamically smooth finish. For
the rough condition of the vertical-tail section, the
model surfaces were the same as for the smooth condition
but 0.002-inch carborundum grains were applied to a thin
layer of shellac on both the upper and lower airfoil
surfaces at various chordwise positions. The roughness
strips were 1.2 inches wide at 0.45c, 0.5 inch wide
at 0.30c, 0.15c, and 0.10c, and 3.75 inches wide at the
leading edge (1.875 in. along each surface measured from
the leading edge).

TESTS

Tests of the three models were made in the Langley
two-dimensional low-turbulence pressure tunnel. The
tests included measurements at a Reynolds number of
approximately 6×10^6 of airfoil lift and drag, control-
surface hinge moment, and balance pressure for each
model with various deflections of the control surfaces.
Observations of the air flow over the surfaces of both
tail sections were made by means of tuft surveys. Lift
and drag measurements were also made at Reynolds numbers
of approximately 3×10^6 and 9×10^6 for the horizontal-
and vertical-tail sections with the control surfaces
neutral. In addition, the vertical-tail section was
tested at a Reynolds number of 6×10^6 with roughness
strips applied to both upper and lower airfoil surfaces
at various chordwise positions. The Mach numbers
corresponding to Reynolds numbers of 3×10^6, 6×10^6,
and 9×10^6 were 0.11, 0.14, and 0.10, respectively.

The following formulas were used to correct the
tunnel data to free-air conditions:

$$c_l = \left[1 - 2\Lambda \left(\sigma + \xi \right) - \sigma \right] c_l'$$

$$c_d = \left[1 - 2\Lambda\left(\sigma + \xi\right)\right]c_d{}'$$

$$a_o = \left(1 + \sigma\right)a_o{}'$$

$$q_o = \left[1 + 2\Lambda\left(\sigma + \xi\right)\right]q_o{}'$$

where

Λ factor dependent on airfoil shape

σ factor dependent on ratio of airfoil size to tunnel height

ξ factor used for correcting effect of model upon velocity measured by static-pressure orifices

and the primed quantities represent the values measured in the tunnel.

The values of $2\Lambda\left(\sigma + \xi\right)$ were 0.0115, 0.00979, and 0.00792 for the wing, vertical-tail, and horizontal-tail sections, respectively. The value of σ was equal to 0.015 for all three airfoils.

RESULTS AND DISCUSSION

Values of the important aerodynamic parameters measured when a_o and δ_x are approximately 0 for the three models tested are presented in the following table:

Airfoil section	Airfoil surface condition	$\left(\dfrac{\delta c_l}{\delta a_o}\right)_{\delta_x}$	$\left(\dfrac{\delta a_o}{\delta \delta_x}\right)_{c_l}$	$\left(\dfrac{\delta c_{h_x}}{\delta a_o}\right)_{\delta_x}$	$\left(\dfrac{\delta c_{h_x}}{\delta \delta_x}\right)_{a_o}$
Rudder	Smooth	0.107	0.58	-0.0034	-0.0007
	L.E. rough	.107	.58	-.0009	-------
Elevator	Smooth	.100	.62	-.0029	-.0023
Aileron	Smooth	.101	.48	-.0004	-.0013

Vertical-Tail Section ·

Lift, hinge-moment, balance-pressure, and drag data for the vertical-tail section with the airfoil surfaces aerodynamically smooth and also with roughness strips applied at various chordwise positions are presented in figures 5 to 14.

Lift.- The lift characteristics of the vertical-tail section at a Reynolds number of approximately 6×10^6 are presented in figure 5 for the airfoil in a smooth condition. The values of $\left(\dfrac{\partial c_l}{\partial a_o}\right)_{\delta_r}$ and $\left(\dfrac{\partial c_l}{\partial \delta_r}\right)_{a_o}$ are equal to 0.107 and 0.062, respectively, and the effectiveness parameter $\left(\dfrac{\partial a_o}{\partial \delta_r}\right)_{c_l}$ is equal to 0.58. The increment of section lift coefficient Δc_l plotted against rudder deflection is presented in figure 6 for four section angles of attack from 0° to 12°. These curves show that for small rudder deflections the effectiveness remains constant through this range of angle of attack. At rudder deflections more negative than -2°, the increment of section lift coefficient increases with decreasing angle of attack until the air flow over the lower surface of the rudder begins to separate. This separation occurs at low angles of attack for high negative rudder deflections as shown in figures 5 and 6 and was observed by means of tuft surveys over the airfoil surfaces.

Scale effect on the lift characteristics is shown in figure 7. Lift measurements were made with the rudder neutral at Reynolds numbers of approximately 3×10^6, 6×10^6, and 9×10^6.

The effect of fixed transition on the lift characteristics at rudder deflections of 0°, -5°, and -10° is shown in figure 8. Application of roughness to the airfoil leading edge caused an average reduction in maximum section lift coefficient of approximately 12 percent but had a negligible effect on the lift-curve slope with the rudder neutral. The values of $\left(\dfrac{\partial c_l}{\partial \delta_r}\right)_{a_o}$

and $\left(\dfrac{\delta \alpha_o}{\delta \delta_r}\right)_{c_l}$ that were obtained between rudder deflections

of -5° and 0° and at zero angle of attack remained the same as for the aerodynamically smooth condition, but the increment of c_l caused by rudder deflections of -5° and -10° decreased at low angles of attack when transition was induced at the airfoil leading edge (fig. 8); the sharp irregularity in the variation of Δc_l with δ_r shown in figure 6 was thereby eliminated.

Hinge moment.- The variation of rudder section hinge-moment coefficient c_{h_r} with airfoil section angle of attack for the smooth airfoil is presented in figure 9 for rudder deflections between -19° and 19° at a Reynolds number of approximately 6×10^6. Corresponding curves of the pressure difference across the rudder balance seal $\Delta p/q_o$ against α_o are presented in figure 11. These data may be used to estimate the hinge-moment characteristics of a rudder of similar contour and chord by the methods of reference 1. For the 41.2-percent sealed internal balance, the values

of $\left(\dfrac{\delta c_{h_r}}{\delta \alpha_o}\right)_{\delta_r}$ and $\left(\dfrac{\delta c_{h_r}}{\delta \delta_r}\right)_{\alpha_o}$ were equal to -0.0034

and -0.0007, respectively, for the airfoil surfaces in a smooth condition.

The sharp irregularities in the curves of c_{h_r} against α_o (fig. 9) correspond to the limits of the low-drag range as shown in figure 13 and are believed to be caused by the sudden movements in transition along the airfoil surfaces at the extremities of the low-drag range. The data of figure 10 were taken at rudder deflections of 0°, -5°, and -10° with transition strips placed on the airfoil surfaces at various chordwise positions to limit the movement of transition. As the fixed transition was moved forward of the $0.15c$ position

the irregularities in $\left(\dfrac{\delta c_{h_r}}{\delta \alpha_o}\right)_{\delta_r}$ diminished in magnitude

but were not entirely removed until transition was fixed

at the airfoil leading edge. The value of $\left(\dfrac{\delta c_{h_r}}{\delta a_o}\right)_{\delta_r}$

with transition fixed at the airfoil leading edge was -0.0009
as compared with -0.0034 for the aerodynamically smooth
airfoil. A forward position of transition had no signifi-
cant effect on the variation of $\Delta p/q_o$ with a_o (fig. 12).

Drag.- Drag characteristics of the vertical-tail
section in a smooth condition are presented in figure 13
at Reynolds number of approximately 3×10^6, 6×10^6,
and 9×10^6 with the rudder neutral and at a Reynolds
number of approximately 6×10^6 with rudder deflections
between -5° and 5°. Through this range of rudder deflec-
tion the value of the minimum section drag coefficient
and the range of lift coefficient for low-drag values
remained substantially the same. Drag polars for the air-
foil section with transition strips applied to the airfoil
surfaces at various chordwise positions are presented in
figure 14 for rudder deflections of 0° and -5°.

Horizontal-Tail Section

Lift, hinge-moment, balance-pressure, and drag data
for the horizontal-tail section with the airfoil surfaces
aerodynamically smooth are presented in figures 15 to 20.

Lift.- The lift characteristics of the horizontal-
tail section at a Reynolds number of approximately 6×10^6
are presented in figure 15 for various elevator deflections

between -23° and 9°. The values of $\left(\dfrac{\delta c_l}{\delta a_o}\right)_{\delta_e}$ and $\left(\dfrac{\delta c_l}{\delta \delta_e}\right)_{a_o}$

are equal to 0.100 and 0.062, respectively, and the

effectiveness parameter $\left(\dfrac{\delta a_o}{\delta \delta_e}\right)_{c_l}$ is equal to 0.62. The

variation of the increment of section lift coefficient Δc_l

with elevator deflection is presented in figure 16 for four
section angles of attack from -4° to 8°. Between elevator
deflections of -3° and 3° the effectiveness remains constant
throughout this range of angle of attack. At elevator
deflections more negative than -3° the increment of section

lift coefficient increases with decreasing section angle
of attack until, as in the case of the rudder, the air
flow over the lower surface of the elevator begins to
separate. This separation, which was observed by means of
tuft surveys over the airfoil surfaces, causes the sharp
breaks in the lift curves of figure 15 and results in the
decreased value of Δc_l at high negative elevator angles
and low angles of attack (fig. 16). At positive elevator
deflections greater than $4°$, the value of Δc_l decreases
with increasing angle of attack.

The effect of Reynolds number between 3×10^6
and 9×10^6 on the lift characteristics of the horizontal-
tail section with the elevator neutral is shown in
figure 17.

Hinge moment.- The elevator section hinge-moment
coefficients plotted against airfoil section angle of
attack are presented in figure 18 for elevator deflections
between $-23°$ and $9°$ at a Reynolds number of approximately
6×10^6. As in the case of the rudder tests, irregulari-
ties in the variation of c_{h_e} with α_o correspond to
the limits of the low-drag range as shown in figure 20
and are believed to be caused by the sudden movements in
transition along the airfoil surfaces at the extremities
of the low-drag range. The value of $\left(\dfrac{\partial c_{h_e}}{\partial \alpha_o}\right)_{\delta_e}$ is equal
to -0.0029 and was obtained at an angle of attack of $-2°$
because one of the jogs in the hinge-moment curve occurs
at a section angle of attack of $0°$. If transition occurs
on the airfoil surfaces at a forward chordwise position
because of surface irregularities or roughness, the magni-
tude of the jogs in the curve of the variation of hinge
moment with angle of attack and the absolute value of
$\left(\dfrac{\partial c_{h_e}}{\partial \alpha_o}\right)_{\delta_e}$ may be expected to decrease in a manner similar
to that of the vertical-tail section. The value of $\left(\dfrac{\partial c_{h_e}}{\partial \delta_e}\right)_{\alpha_o}$
for the aerodynamically smooth horizontal-tail section is
approximately -0.0023.

The variation of the pressure difference across the elevator balance seal with a_o is presented in figure 19 at the same elevator deflections for which hinge-moment data are presented. The hinge-moment and seal-pressure data may be used to estimate the hinge-moment characteristics of an elevator of similar contour and chord with any amount of sealed internal balance by the methods of reference 1.

Drag.- Drag characteristics of the horizontal-tail section are presented in figure 20. These data include drag polars at Reynolds number of approximately 3×10^6, 6×10^6, and 9×10^6 with the elevator neutral and at a Reynolds number of 6×10^6 with the elevator deflected $\pm 2^o$.

Wing Section

Lift, hinge-moment, balance-pressure, and drag data for the wing section with the airfoil surfaces aerodynamically smooth are presented in figures 21 to 25.

Lift.- The lift characteristics of the airfoil section with an aileron are presented in figure 21. The values of $\left(\dfrac{\partial c_l}{\partial a_o}\right)_{\delta_a}$ and $\left(\dfrac{\partial c_l}{\partial \delta_a}\right)_{a_o}$ are equal to 0.101 and 0.048, respectively. The effectiveness parameter $\left(\dfrac{\partial a_o}{\partial \delta_a}\right)_{c_l}$ is equal to 0.48 or 84 percent of the thin airfoil theoretical effectiveness (reference 2) and is approximately the same as the effectiveness obtained on the NACA 0009 airfoil section (reference 3).

In order to show the variation of aileron effectiveness with lift coefficient and aileron deflection, values of the effectiveness have been measured between definite aileron deflections. This effectiveness parameter is designated $\left(\dfrac{\Delta a_o}{\Delta \delta_a}\right)_{c_l}$. Curves of $\left(\dfrac{\Delta a_o}{\Delta \delta_a}\right)_{c_l}$ against c_l for various aileron deflection limits are presented in

figure 22.   A comparison of the measured effectiveness between $\delta_a = 0°$ and $10°$ and $\delta_a = 0°$ and $-10°$ shows that the aileron is more effective for negative aileron deflections.   A comparison of the measured effectiveness between $\delta_a = 0°$ and $17°$ and $\delta_a = 0°$ and $-17°$ also shows a higher effectiveness for negative aileron deflections except through an approximate range of section lift coefficient from 0 to 0.3 in which the effectiveness of the down aileron was about the same as that of the up aileron.   At the section lift coefficients greater than approximately 0.4 the effectiveness of the aileron deflected down $17°$ decreased appreciably.   This large decrease in effectiveness at high positive aileron deflections and section angles of attack, probably caused by separation of the air flow over the upper surface of the aileron, is reflected in a decrease in the effectiveness from $\delta_a = \pm10°$ to $\delta_a = \pm17°$.   At section lift coefficients from -0.4 to 0.4 the effectiveness between the limits of $\delta_a = \pm17°$ was almost the same as that measured between the limits of $\delta_a = \pm10°$.   The value of $\left(\dfrac{\Delta a_o}{\Delta \delta_a}\right)_{c_l}$ when measured between $\delta_a = \pm10°$ decreased

from 0.50 at a section lift coefficient of 0 to 0.48 at a section lift coefficient of 0.70 or only 4 percent and, when measured between $\delta_a = 17°$ and $\delta_a = -17°$ decreased from 0.50 to 0.45 or 10 percent over the same lift-coefficient range.

Hinge moment.- The variations of aileron section hinge-moment coefficient c_{h_a} with section angle of attack a_o for all aileron deflections tested are presented in figure 23(a).

The irregularities in $\left(\dfrac{\partial c_{h_a}}{\partial a_o}\right)_{\delta_a}$ shown by these curves are probably caused by the sudden movements in transition on the upper and lower airfoil surfaces at the extremities of the low-drag range. (See fig. 25.)   No sharp irregularities are apparent, however, in the

variation of c_{h_a} with aileron deflection as shown by the

curves of figure 23(b).   The values of $\left(\dfrac{\partial c_{h_a}}{\partial \alpha_o}\right)_{\delta_a}$

and $\left(\dfrac{\partial c_{h_a}}{\partial \delta_a}\right)_{\alpha_o}$ are 0.0004 and -0.0013, respectively,

for the aerodynamically smooth airfoil.

The variation of the pressure difference across the
aileron balance seal $\Delta p/q_o$ with α_o is presented in
figure 24 for all aileron deflections tested. The basic
data of figures 23(a) and 24 may be used to estimate the
section characteristics of an aileron of similar contour
and chord with any amount of sealed internal balance by
the methods of reference 1.

Drag.- The variation of section drag coefficient with
section lift coefficient at a Reynolds number of approxi-
mately 6×10^6 for aileron deflections of 0°, 5°, and -5°
is presented in figure 25. The minimum section drag
coefficient was approximately the same for the three
aileron deflections, although the extent of the low-drag
range was reduced with the aileron deflected $\pm 5^o$ to about
one-half the range with the aileron neutral.

Effects of Sudden Movement of Transition on

Airplane Control-Surface Characteristics

The two-dimensional data presented herein show sudden
changes in the variation of control-surface section hinge-
moment coefficient with airfoil section angle of attack
when transition suddenly moves forward along the airfoil
surfaces. The effect of sudden movements of transition
on the airplane control forces was investigated. In
order to determine whether the irregularities in the two-
dimensional hinge-moment characteristics would cause
unusual aileron wheel-force characteristics, the variation
of wheel force F_w with wing-tip helix angle pb/2V for
an assumed airplane was estimated for various indicated
airspeeds (fig. 26). The values of pb/2V were estimated
from the following equation presented in reference 4:

$$\frac{pb}{2V} = \frac{C_{l_\delta}}{k} \frac{k \, \Delta\delta_a}{114.6 \, C_{l_p}} \tag{1}$$

Test values of $\Delta\alpha_o$ were substituted in equation (1) for the product $k \, \Delta\delta_a$, and values of $\frac{C_{l_\delta}}{k}$ and C_{l_p} equal to 0.331 and 0.495, respectively, were obtained from reference 4 by use of the following assumed airplane dimensions:

Wing span, feet 70.5
Wing area, square feet 554
Wing loading, pounds per square foot 45
Aspect ratio 9
Taper ratio 3
Aileron span, feet 11.5
Aileron root-mean-square chord behind
  hinge axis, feet 1.8
Aileron location, fraction of semispan
   Inboard end 0.668
   Outboard end 1.000
Wheel diameter, feet 1.083
Maximum wheel deflection, degrees . . . . ±175

Wheel forces were estimated from the equation

$$F_w = \frac{q_o b_a \bar{c}_a^2}{\text{Wheel radius}} \left[\left(\frac{d\delta_a}{d\theta}\right)_{up} \left(c_{h_a}\right)_{up} - \left(\frac{d\delta_a}{d\theta}\right)_{down} \left(c_{h_a}\right)_{down} \right] \tag{2}$$

The aileron hinge-moment coefficients $\left(c_{h_a}\right)_{up}$ and $\left(c_{h_a}\right)_{down}$ were estimated from the section data for the airplane in a steady roll. Values of these coefficients were taken at given aileron angles and corrected for the change in angle of attack at the aileron midspan caused by the roll. Equal up and down aileron deflections and a maximum wheel deflection of 175° were used.

Because the values of pb/2V were not corrected for wing twist, control-system stretch, or adverse yaw and the section hinge-moment coefficients were not corrected for

aspect-ratio effects, the estimated values of pb/2V
and F_W are not quantitatively accurate. The values are
useful, however, to show the qualitative variation of
wheel force with wing-tip helix angle.

No sudden changes in the estimated variation of F_W
with pb/2V are apparent in figure 26, which indicates
that inclusion of the hinge moments due to the deflection
of both ailerons tends to eliminate the irregularities in
the hinge-moment variation with angle of attack alone.
If the angle of attack were varied with the ailerons
neutral, however, both the right and left ailerons would
tend to move in the same direction when the change in
angle of attack causes transition to move forward suddenly,
and the effect would be absorbed in the aileron rigging
with no change in the wheel force.

Data recently obtained in the Langley stability
tunnel indicate that sudden movements of transition
cause irregularities in the variation of hinge-moment
coefficient with angle of attack in three-dimensional
flow as well as in two-dimensional flow. Sudden move-
ments of transition along the surfaces of vertical- or
horizontal-tail sections, therefore, will probably cause
sudden changes in rudder or elevator hinge moments. The
data obtained with transition fixed at various locations
along the airfoil surfaces, however, indicate a decrease
in the severity of the jogs in the variation of c_{h_x}

with α_0 as the location of transition is moved toward
the airfoil leading edge. Sudden changes in elevator and
rudder forces, therefore, seem less likely to occur on
an airplane since the full extent of laminar flow on
production airplanes has not been realized because of
manufacturing irregularities and surface deterioration in
service and because transition is induced near or at the
leading edge of tail surfaces that are located within the
propeller slipstream or wing and fuselage wake.

CONCLUDING REMARKS

Results of a two-dimensional wind-tunnel investigation
of a low-drag vertical-tail, horizontal-tail, and wing
section equipped with sealed internally balanced control
surfaces have been presented. Sharp irregularities
occurred in the variation of the control-surface section

hinge-moment coefficient with section angle of attack,
which were probably caused by sudden movements in transi-
tion along the surfaces of the airfoils at the extremities
of the low-drag range. Tests of the vertical-tail section
indicated that these irregularities were reduced in magni-
tude when transition was fixed at a forward chordwise
position but were not entirely removed until transition
was fixed at the airfoil leading edge. An estimated varia-
tion of aileron wheel force with wing-tip helix angle for
an assumed airplane indicated that no unusual aileron
wheel-force characteristics would be caused by the
irregularities in the two-dimensional hinge-moment charac-
teristics. Sudden changes in rudder or elevator hinge
moments, however, would probably result from sudden move-
ments in transition along the surfaces of the vertical- or
horizontal-tail sections. If transition should occur at
or near the leading edge of the tail surfaces, as is
usually the case for tail surfaces located within the
propeller slipstream or wing and fuselage wake, no sudden
changes would occur in the control-surface hinge moments.

Langley Memorial Aeronautical Laboratory
       National Advisory Committee For Aeronautics
             Langley Field, Va., March 8, 1946

REFERENCES

1. Fischel, Jack: Hinge Moments of Sealed-Internal-
       Balance Arrangements for Control Surfaces.
       II - Experimental Investigation of Fabric Seals
       in the Presence of a Thin-Plate Overhang. NACA
       ARR No. L5F30a, 1945.

2. Glauert, H.: Theoretical Relationships for an
       Aerofoil with Hinged Flap. R. & M. No. 1095,
       British A.R.C., 1927.

3. Ames, Milton B., Jr., and Sears, Richard I.: Deter-
       mination of Control-Surface Characteristics from
       NACA Plain-Flap and Tab Data. NACA Rep. No. 721,
       1941.

4. Gilruth, R.R., and Turner, W.N.: Lateral Control
       Required for Satisfactory Flying Qualities Based
       on Flight Tests of Numerous Airplanes. NACA
       Rep. No. 715, 1941.

c = 24

$c_b = 0.412c_r$ $c_r = 0.40c$

Maximum length line   Hinge axis

.005c gap normal to rudder nose,
both surfaces

Vertical-tail section

c = 24

$c_b = 0.43c_e$ $c_e = 0.35c$

Maximum length line   Hinge axis

.02850c

Horizontal-tail reference line   7.5°

0.005c gap normal to elevator nose,
both surfaces

.01083c

Horizontal-tail section

.0052c gap normal to aileron nose,
both surfaces

.00849c

Wing reference line   Hinge axis   .04235c

Maximum length line

c = 24 $c_b = .44c_a$ $c_a = 0.22c$
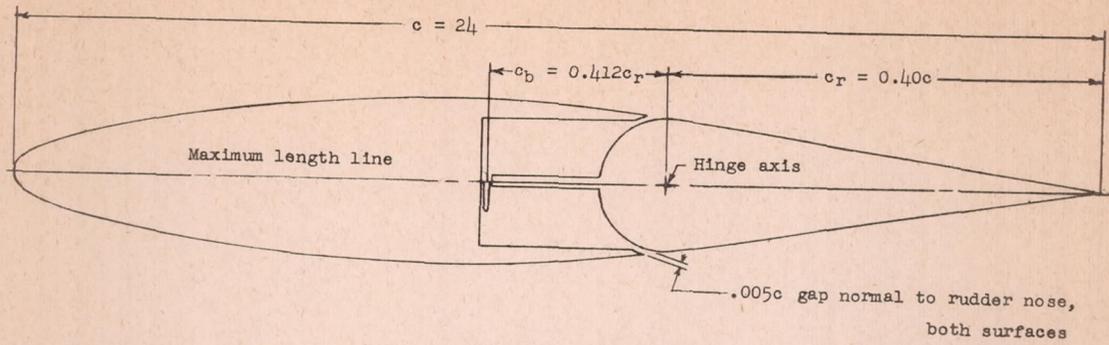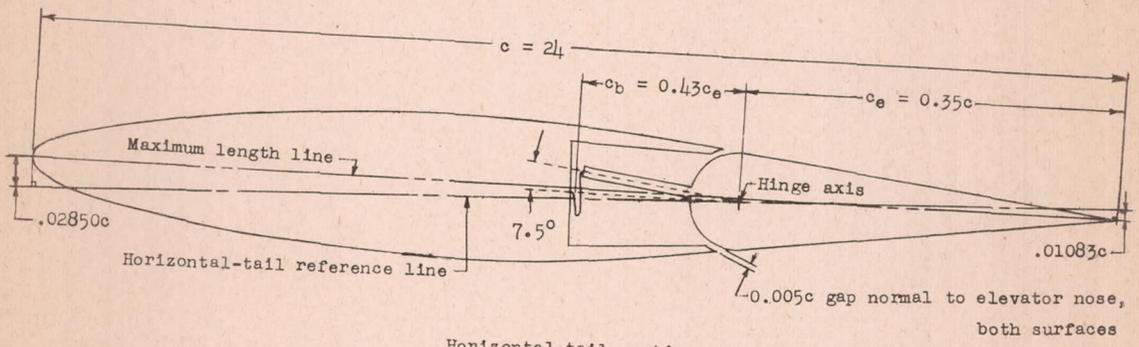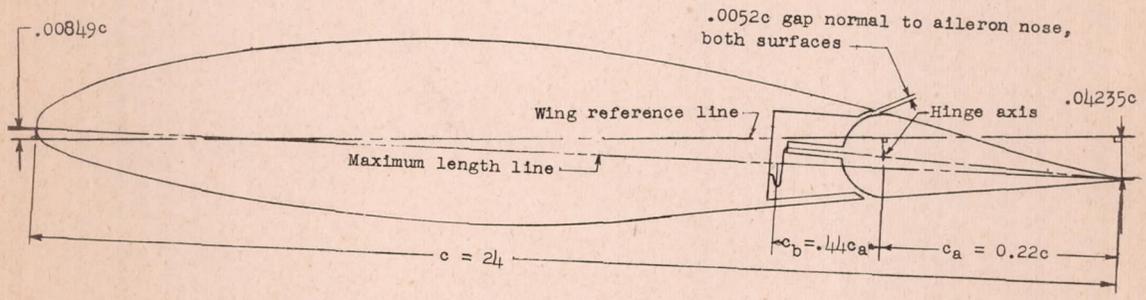
Wing section

Figure 1.- Vertical-tail, horizontal-tail, and wing sections.

Fig. 2   NACA TN No. 1048
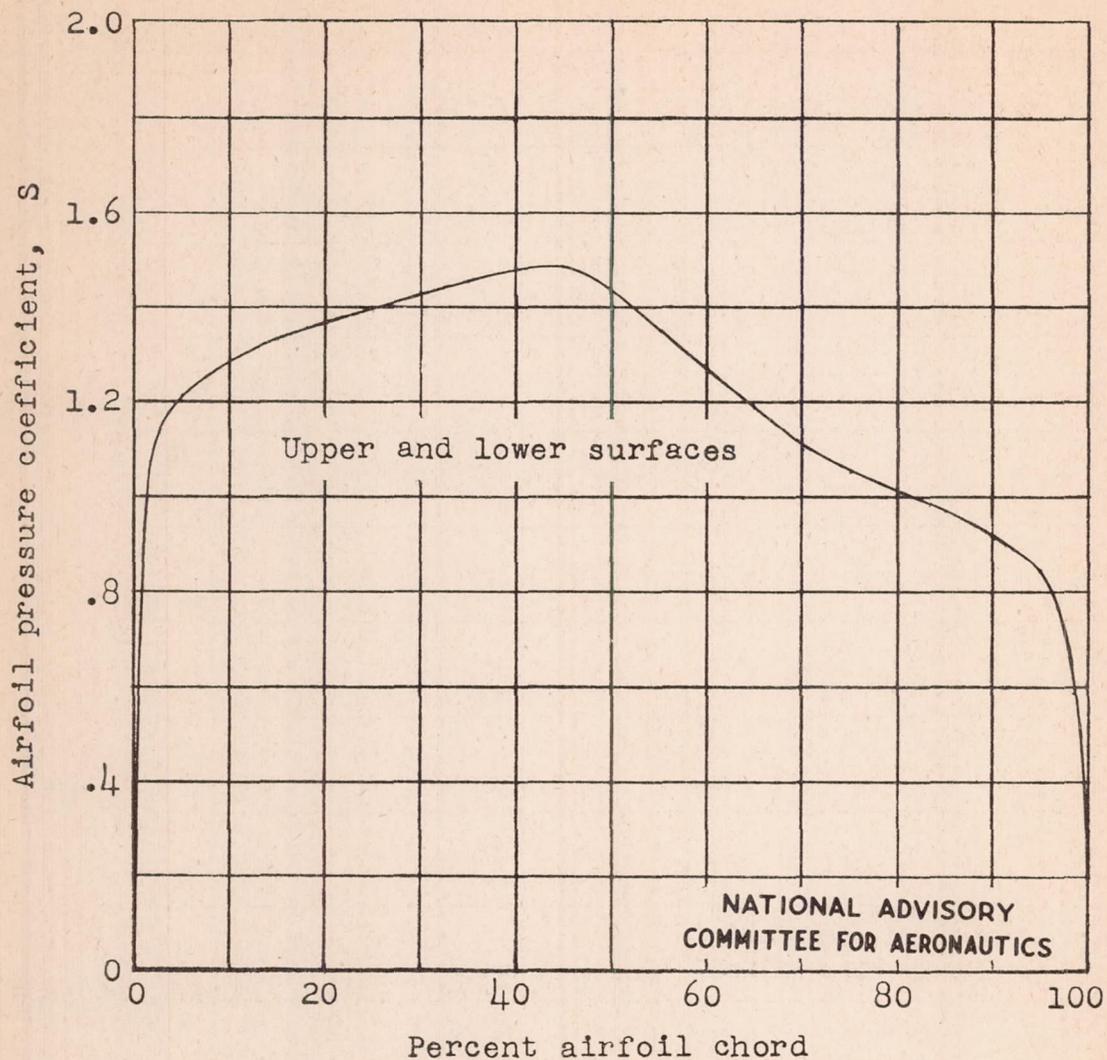
Figure 2.-   Theoretical pressure distribution at zero
     lift of the low-drag vertical-tail section.
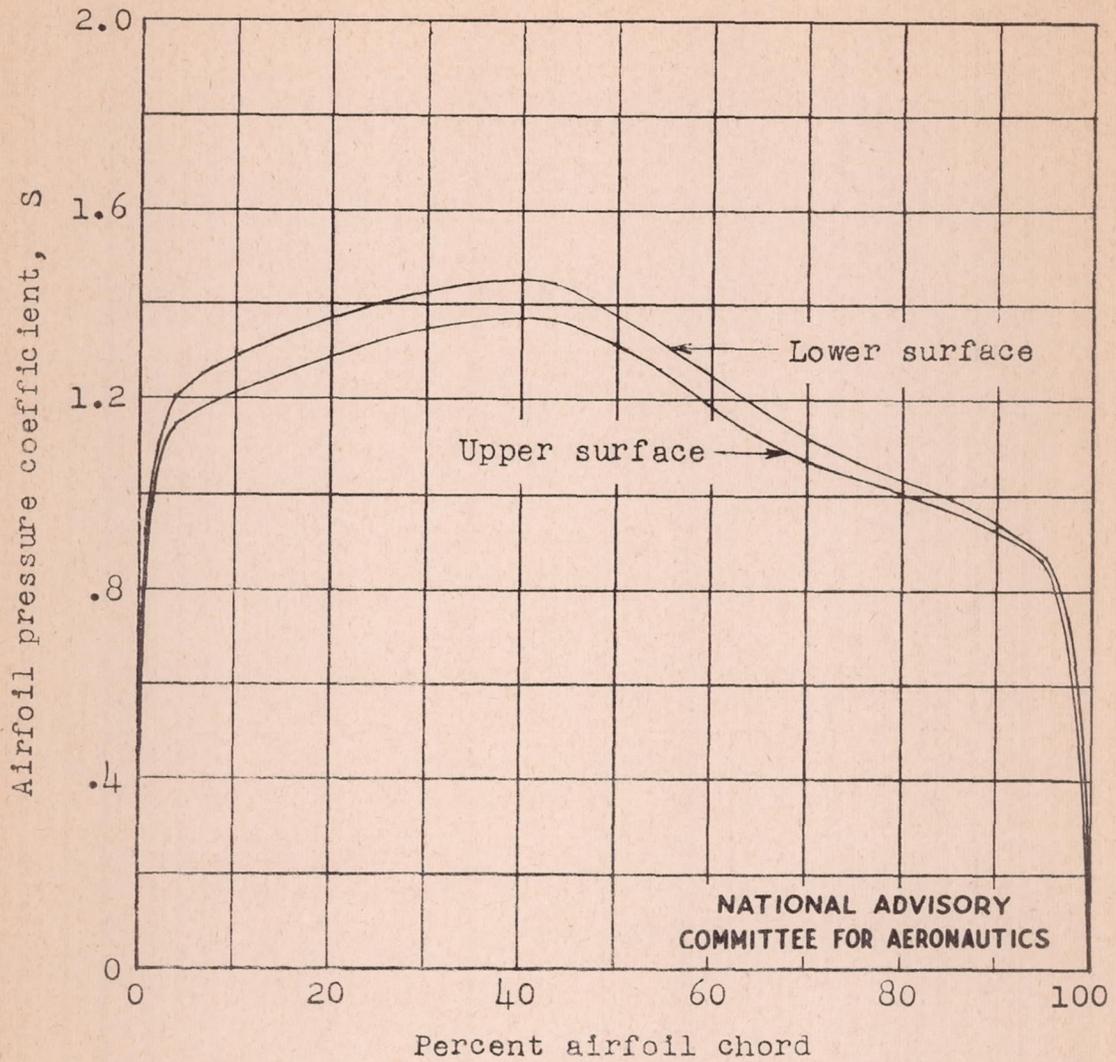
Figure 3.-   Theoretical pressure distribution at a
    section lift coefficient of -0.053 of the low-drag
    horizontal-tail section.

Fig. 4   NACA TN No. 1048
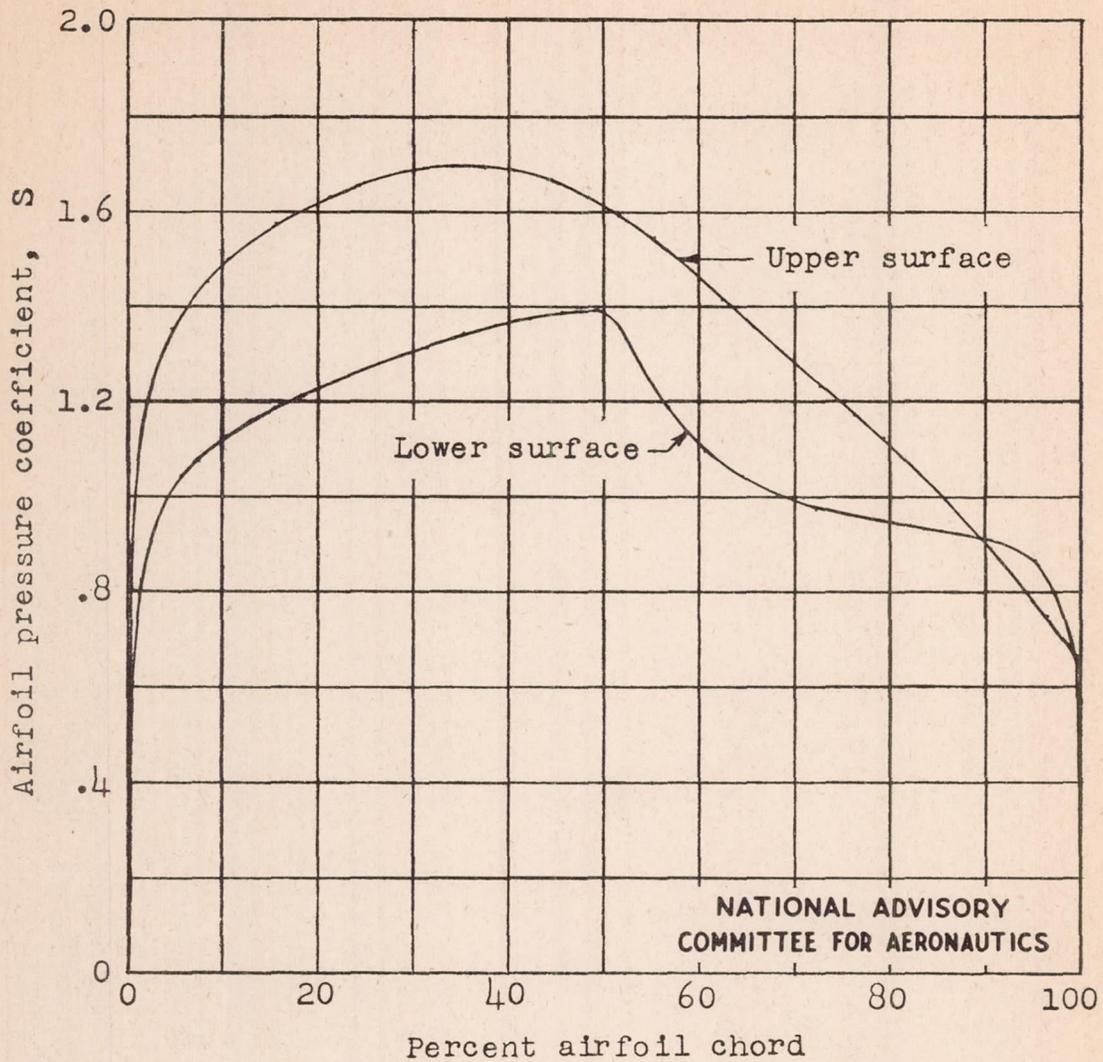
Figure 4.- Theoretical pressure distribution at a section lift coefficient of 0.266 of the low-drag wing section.
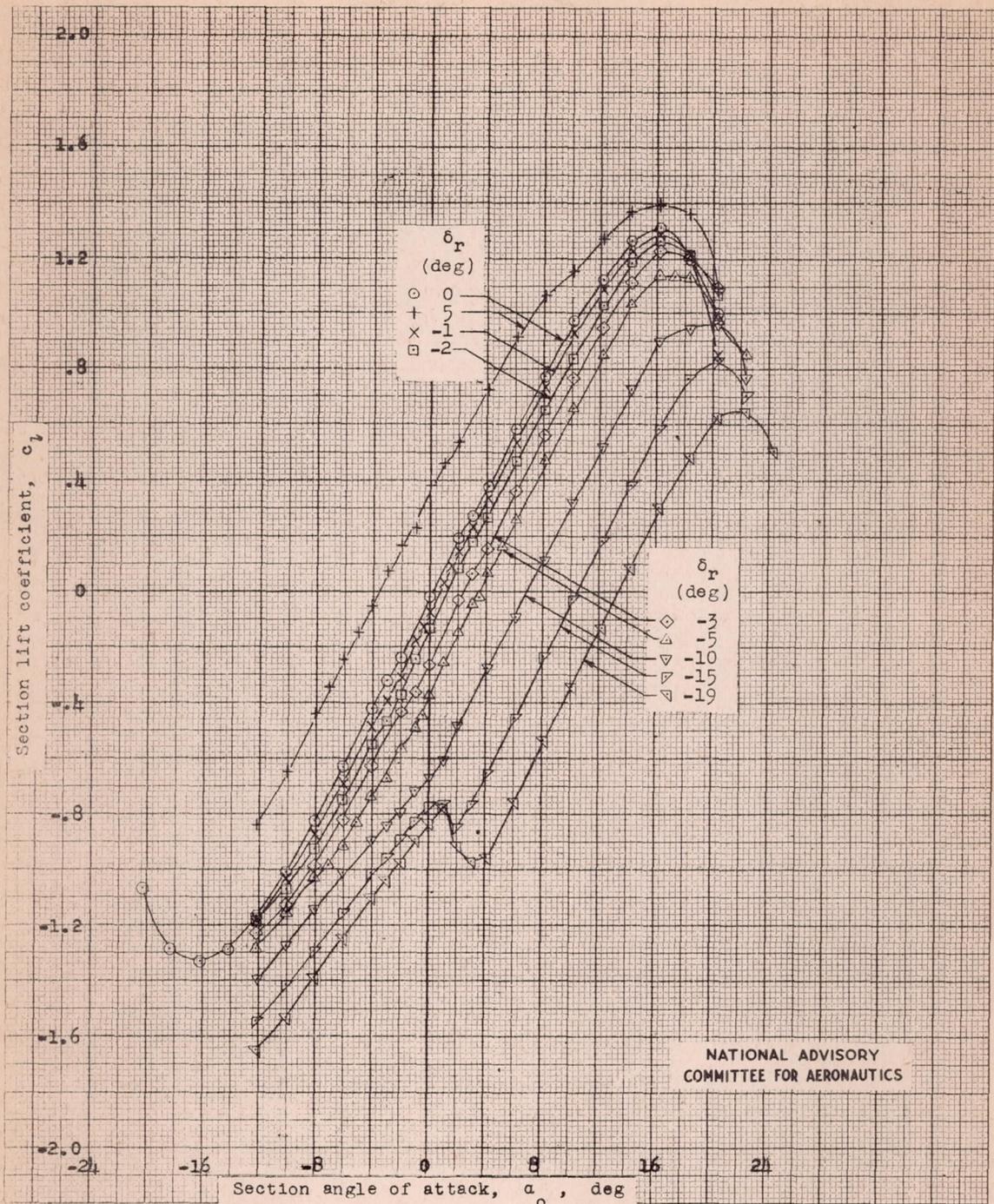
Figure 5.- Lift characteristics of a low-drag vertical-tail section
equipped with a 0.40c sealed internally balanced rudder.　Smooth
condition; R = 6 × 10⁶ (approx.); test, TDT 582.

Fig. 6
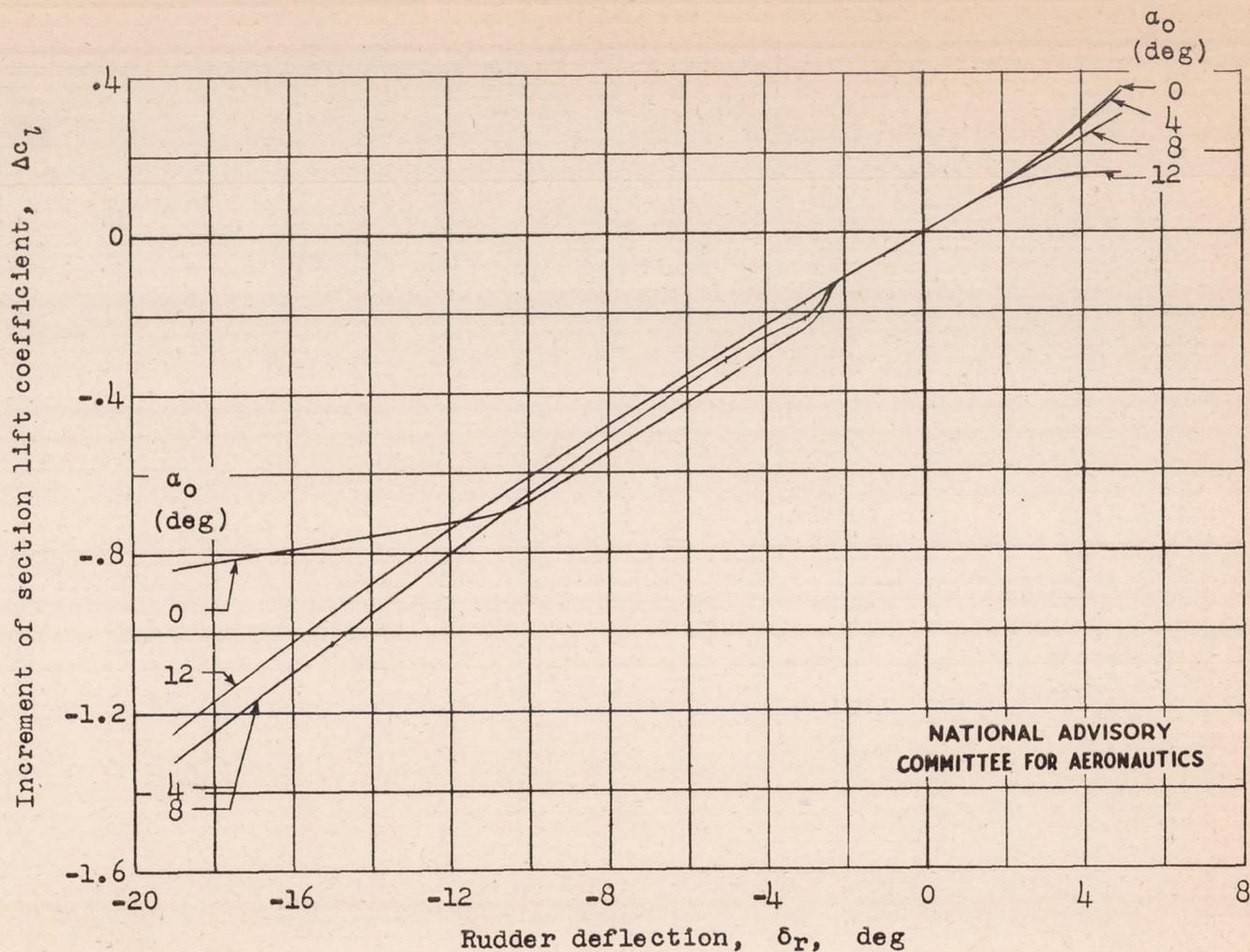
Figure 6.- Variation of Δc_l with δ_r at constant α_o for a low-drag vertical-tail section equipped with a 0.40c sealed internally balanced rudder. Smooth condition; $R = 6 \times 10^6$ (approx.).
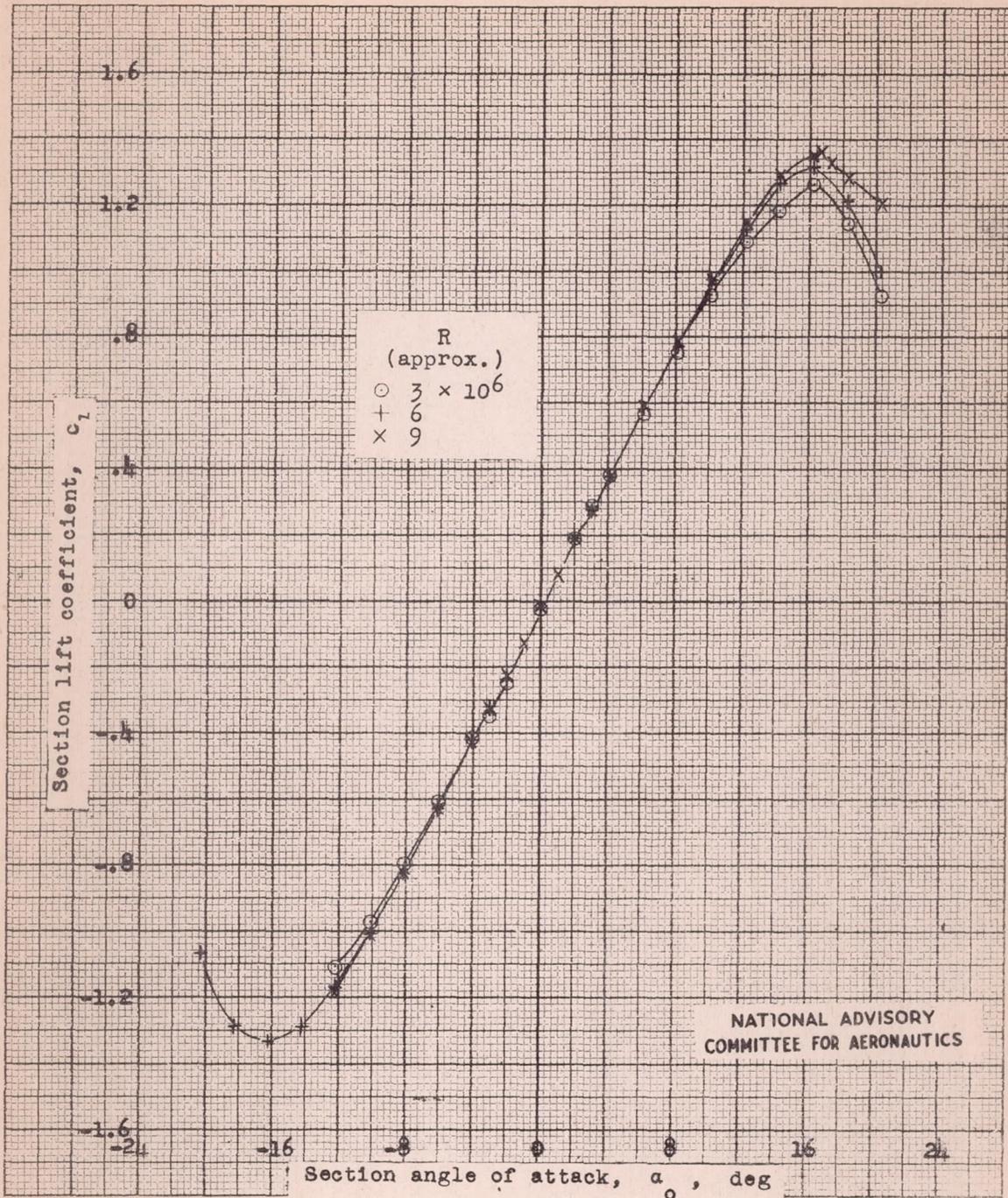
Figure 7.- Lift characteristics of a low-drag vertical-tail section
equipped with a 0.40c sealed internally balanced rudder.
Smooth condition; $\delta_r = 0°$; test, TDT 582.

Fig. 8   NACA TN No. 1048
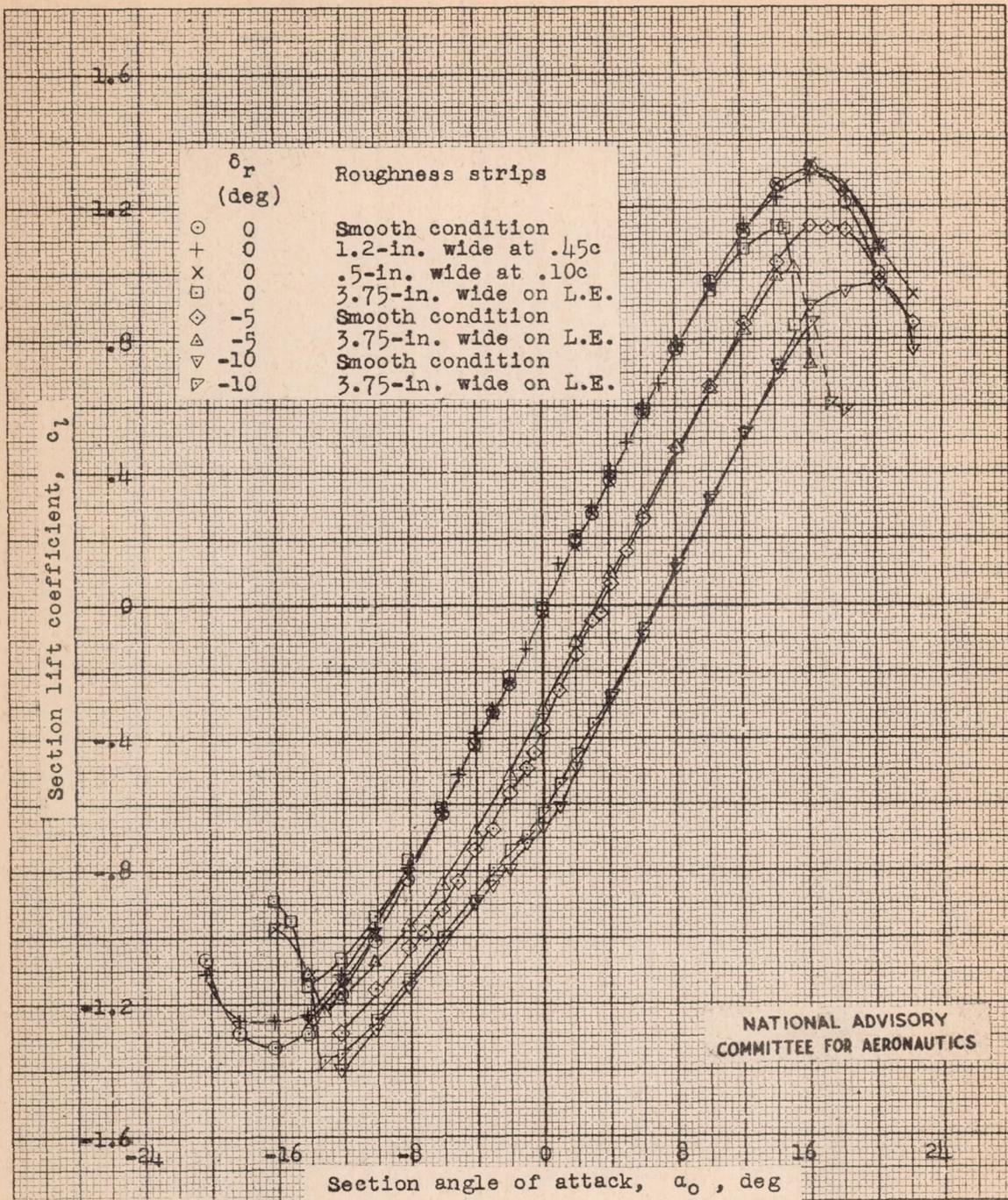
Figure 8.- Lift characteristics of a low-drag vertical-tail section
equipped with a 0.40c sealed internally balanced rudder.
Strips of 0.002-inch carborundum grains on both airfoil
surfaces at various chordwise positions; $R = 6 \times 10^6$ (approx.);
test, TDT 585.
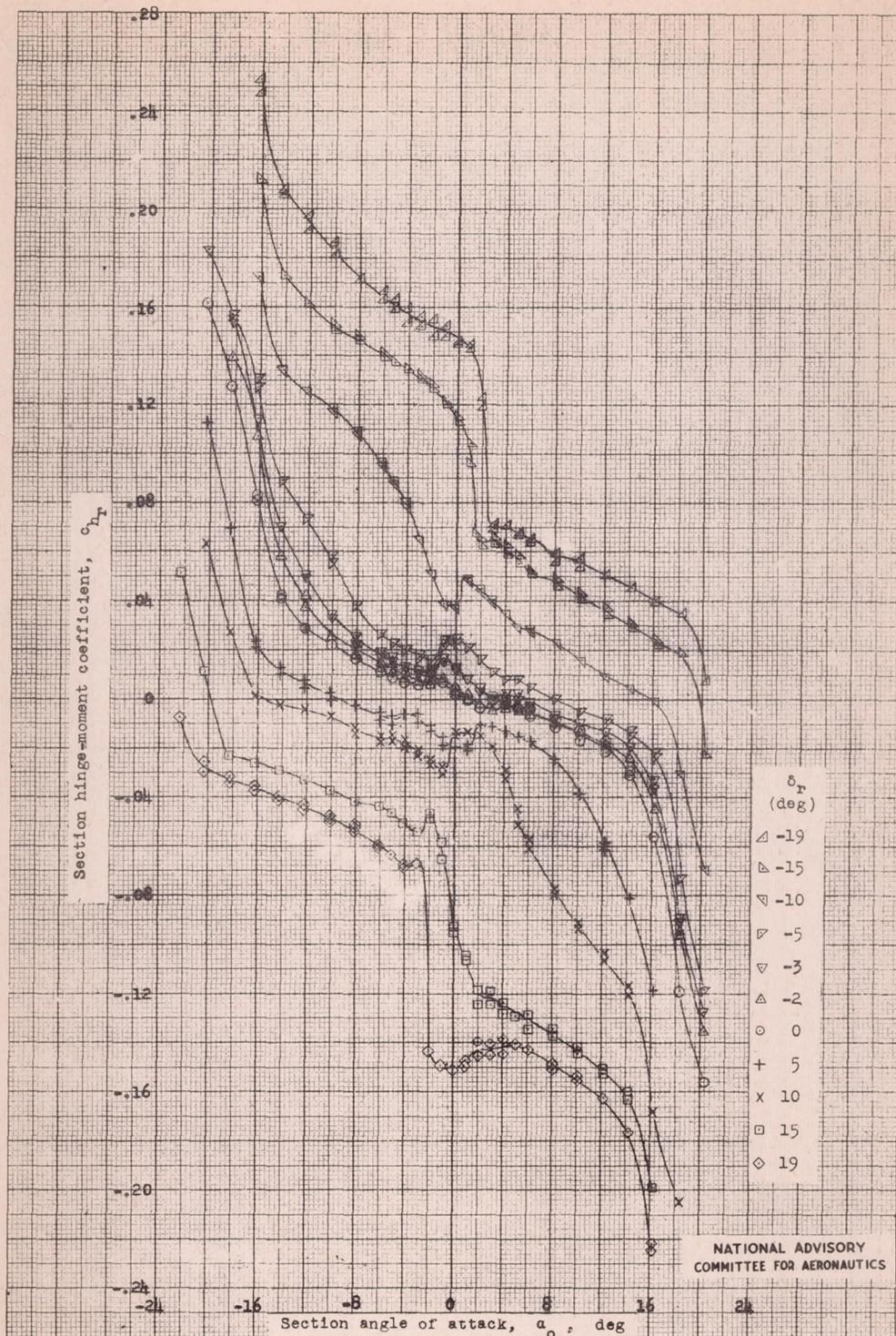
Figure 9.- Hinge-moment characteristics of a 0.40c sealed internally
balanced rudder on a low-drag vertical-tail section.   Smooth
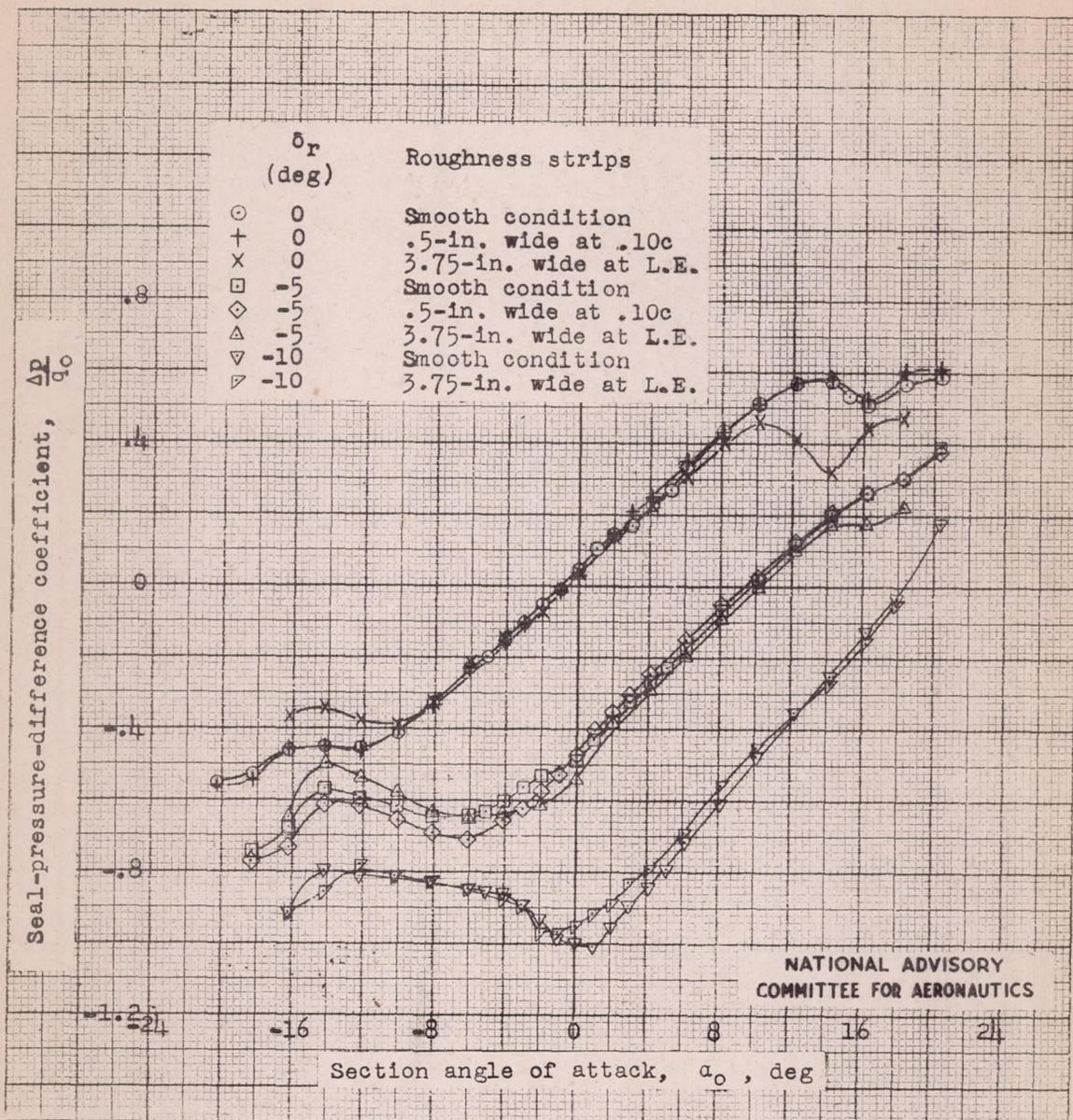condition; R = 6 × 10⁶ (approx.); test, TDT 584.

Section hinge-moment coefficient, c_{h_r}

Section hinge-moment coefficient, c_{h_r}

.20

.16

.12

.08

.04

0

-.04

-.08

-.12

-.16

Roughness strips

⊙ Smooth condition
+ 1.2-in. wide at .45c
× .5-in. wide at .30c

Roughness strips

☐ .5-in. wide at .15c
◇ .5-in. wide at .10c
△ 3.75-in. wide at L.E.

NATIONAL ADVISORY
COMMITTEE FOR AERONAUTICS

-24   -16   -8   0   8   16   24

Section angle of attack, α_o , deg

Section angle of attack, α_o , deg

(a) $\delta_r = 0°$.
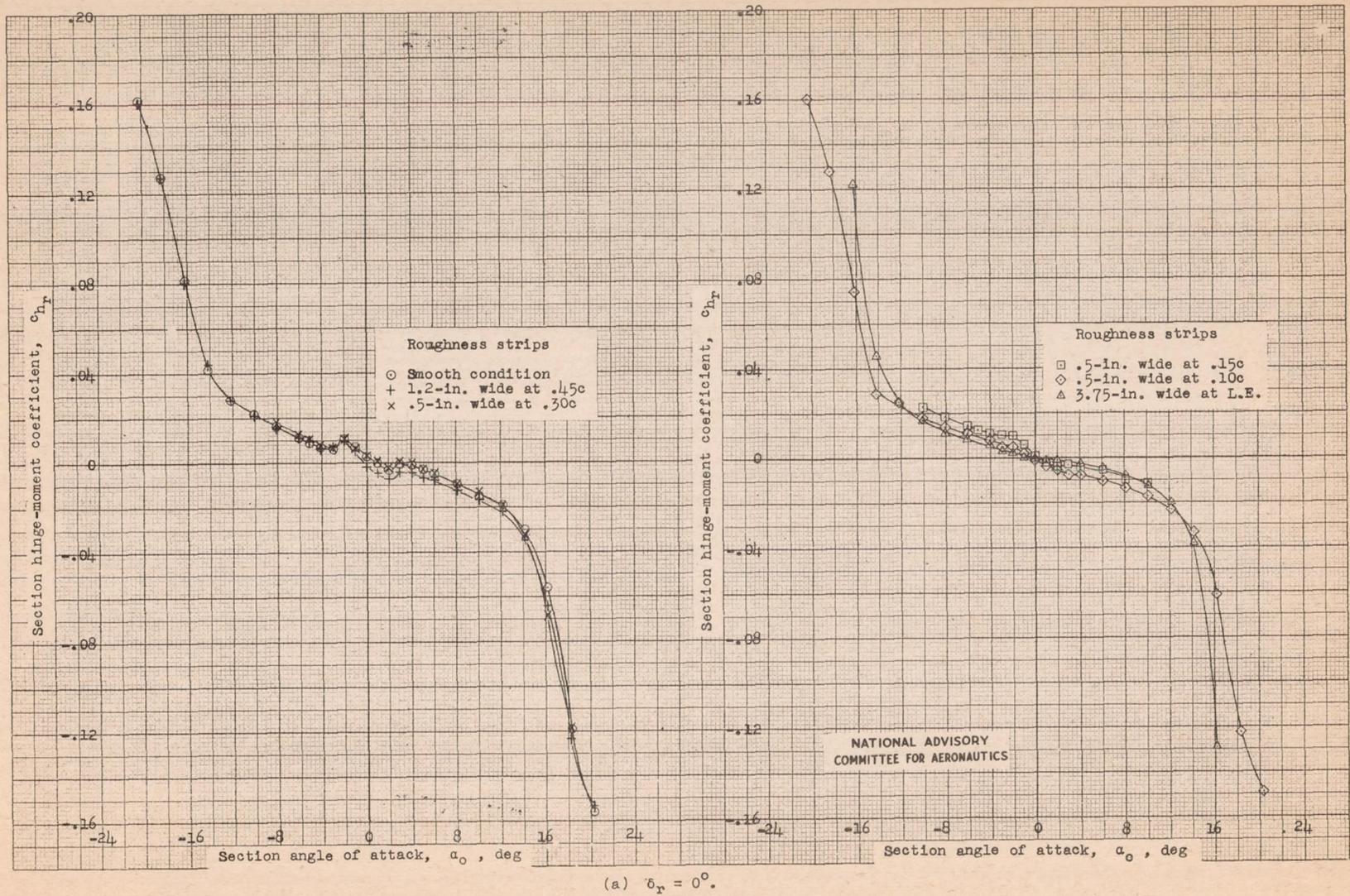
Figure 10.- Hinge-moment characteristics of a 0.40c sealed internally balanced rudder on a low-drag vertical-tail
section. Strips of 0.002-inch carborundum grains on both airfoil surfaces at various chordwise positions;
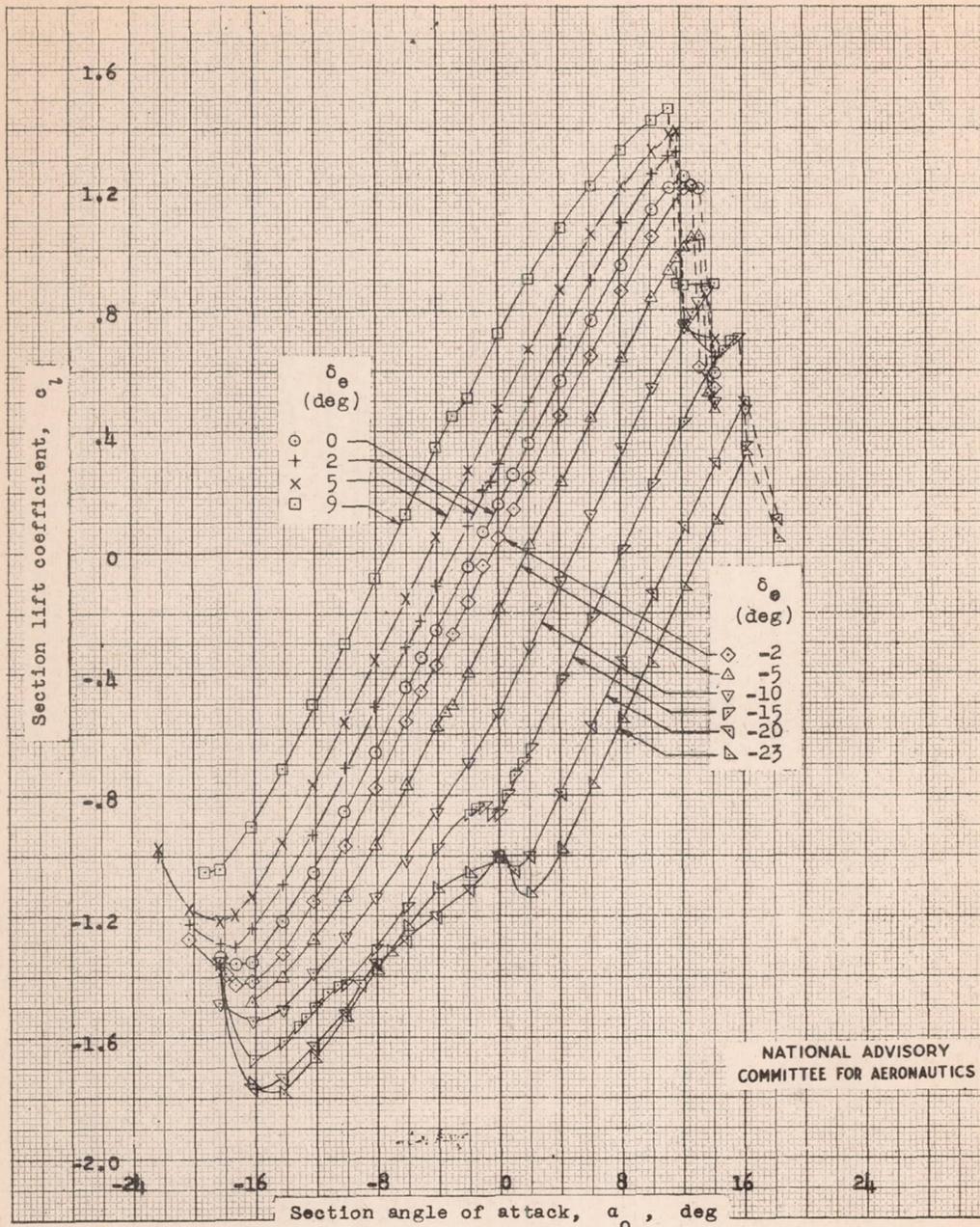$R = 6 \times 10^6$ (approx.); test, TDT 585.

Roughness strips

⊙ Smooth condition
+ 1.2-in. wide at .45c
× 3.75-in. wide at L.E.

Roughness strips

□ Smooth condition
◇ 3.75-in. wide at L.E.

NATIONAL ADVISORY
COMMITTEE FOR AERONAUTICS

(b) $\delta_r = -5°$.
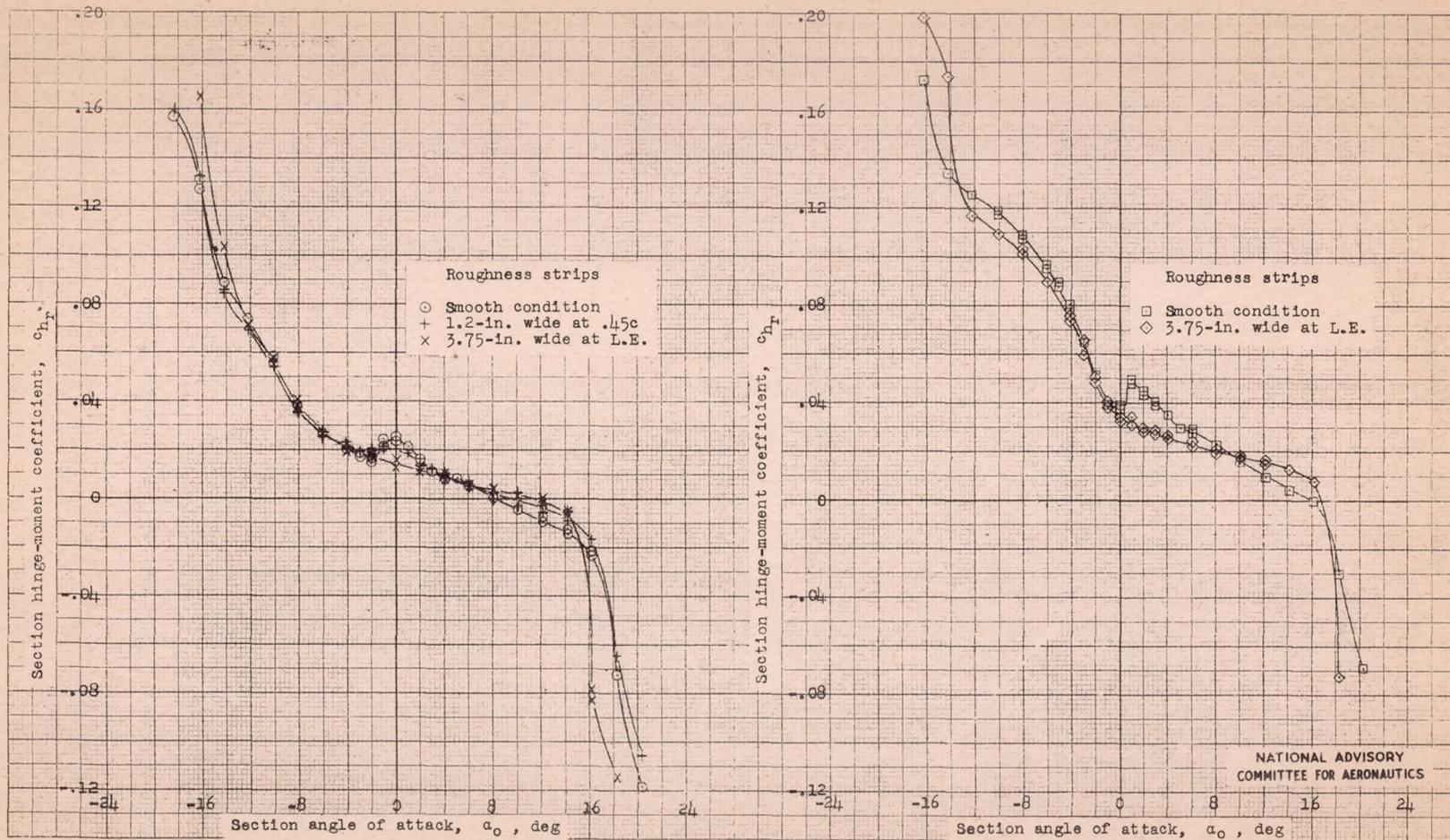
(c) $\delta_r = -10°$.

Figure 10.- Concluded.

Fig. 11   NACA TN No. 1048
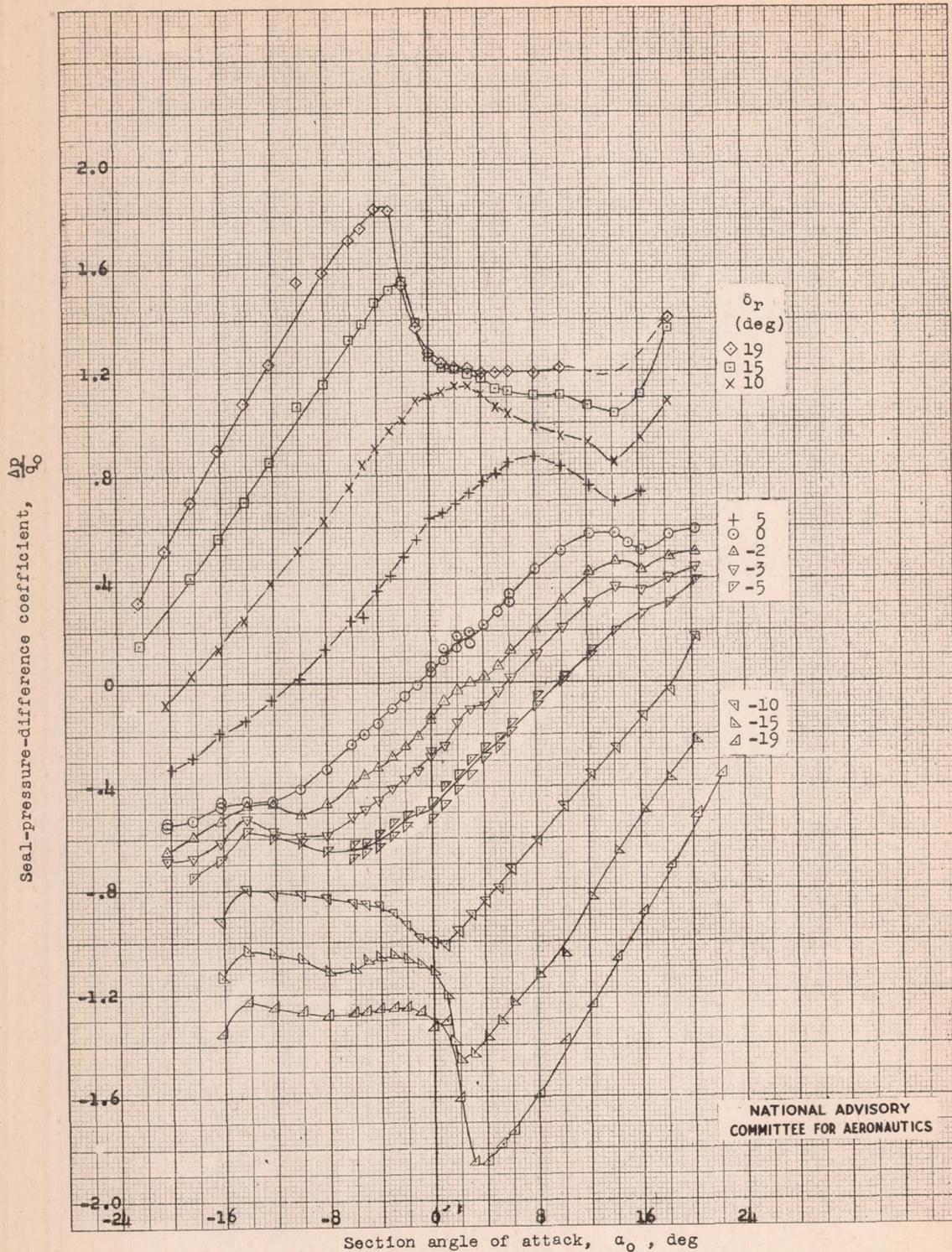
Figure 11.- Variation of $\frac{\Delta p}{q_o}$ with α_o for a 0.40c sealed internally balanced rudder on a low-drag vertical-tail section. Smooth condition; $R = 6 \times 10^6$ (approx.); test, TDT 584.

Figure 12.— Variation of $\frac{\Delta p}{q_o}$ with a_o for a 0.40c sealed internally balanced rudder on a low-drag vertical-tail section. Strips of 0.002-inch carborundum grains on both airfoil surfaces at various chordwise positions; $R = 6 \times 10^6$ (approx.); test, TDT 585.

Fig. 13
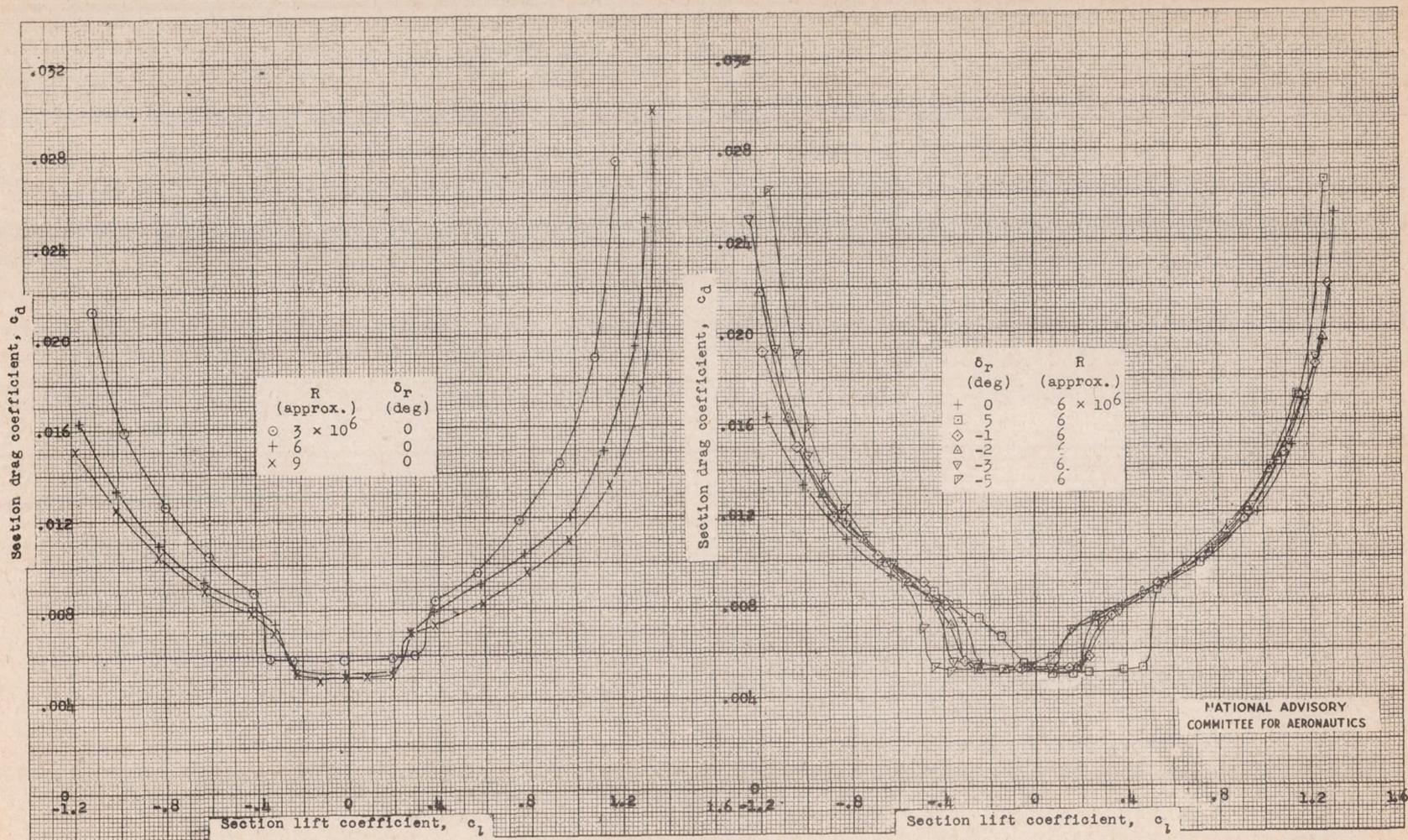
Figure 13.- Drag characteristics of a low-drag vertical-tail section equipped with a
0.40c sealed internally balanced rudder.   Smooth condition; test TDT 582.
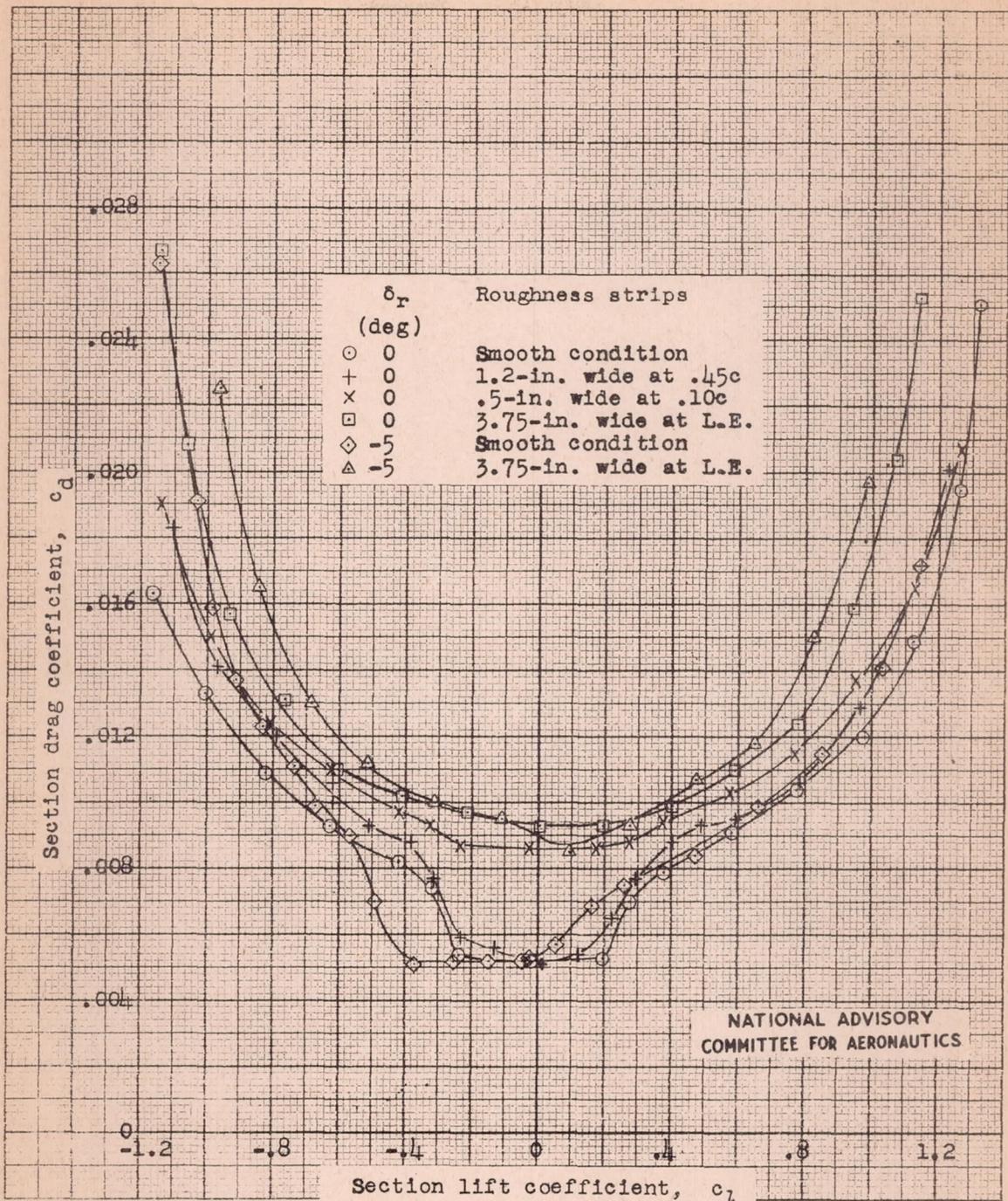
Figure 14.- Drag characteristics of a low-drag vertical-tail
    section equipped with a 0.40c sealed internally balanced
    rudder.   Strips of 0.002-inch carborundum grains on both
    airfoil surfaces at various chordwise positions;
    $R = 6 \times 10^6$ (approx.); test, TDT 585.

Fig. 15

NACA TN No. 1048

Figure 15.- Lift characteristics of a low-drag horizontal-tail section
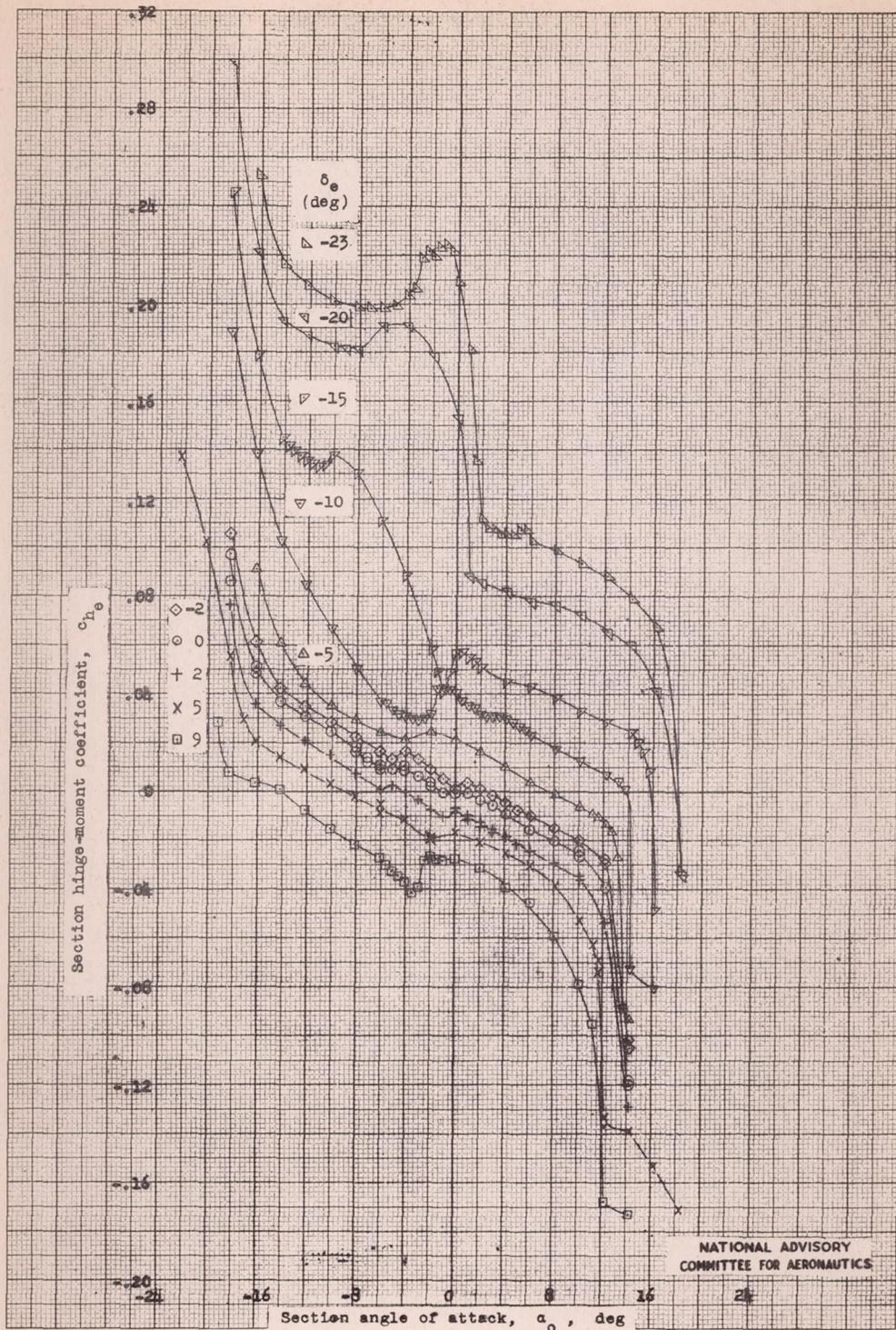equipped with a 0.35c sealed internally balanced elevator.
R = 6 × 10⁶ (approx.); tests, TDT 581 and 589.

Fig. 16
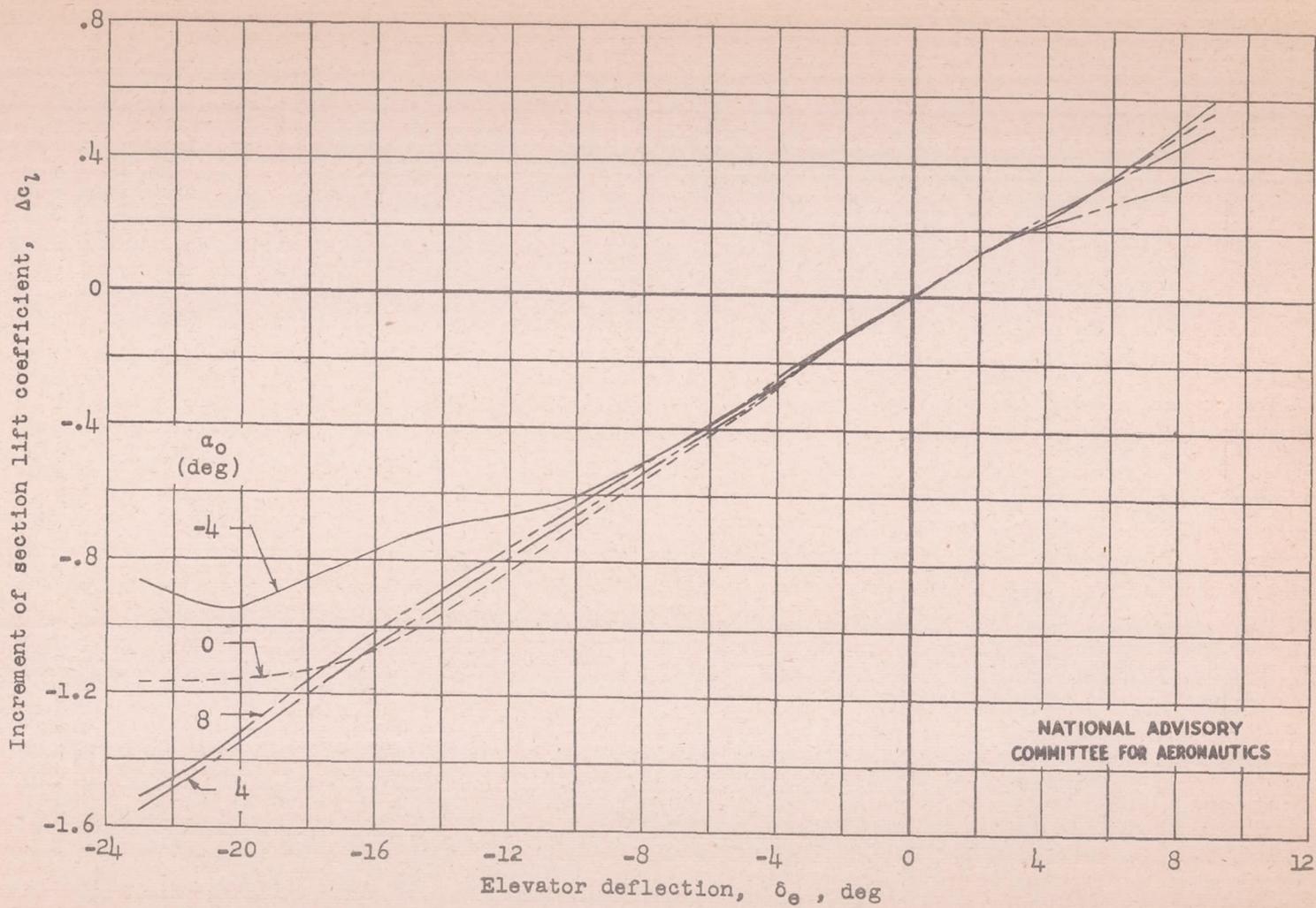
Figure 16.- Variation of Δc_l with δ_e at constant α_o for a low-drag horizontal-tail section equipped with a 0.35c sealed internally balanced elevator. $R = 6 \times 10^6$ (approx.).

Fig. 17   NACA TN No. 1048
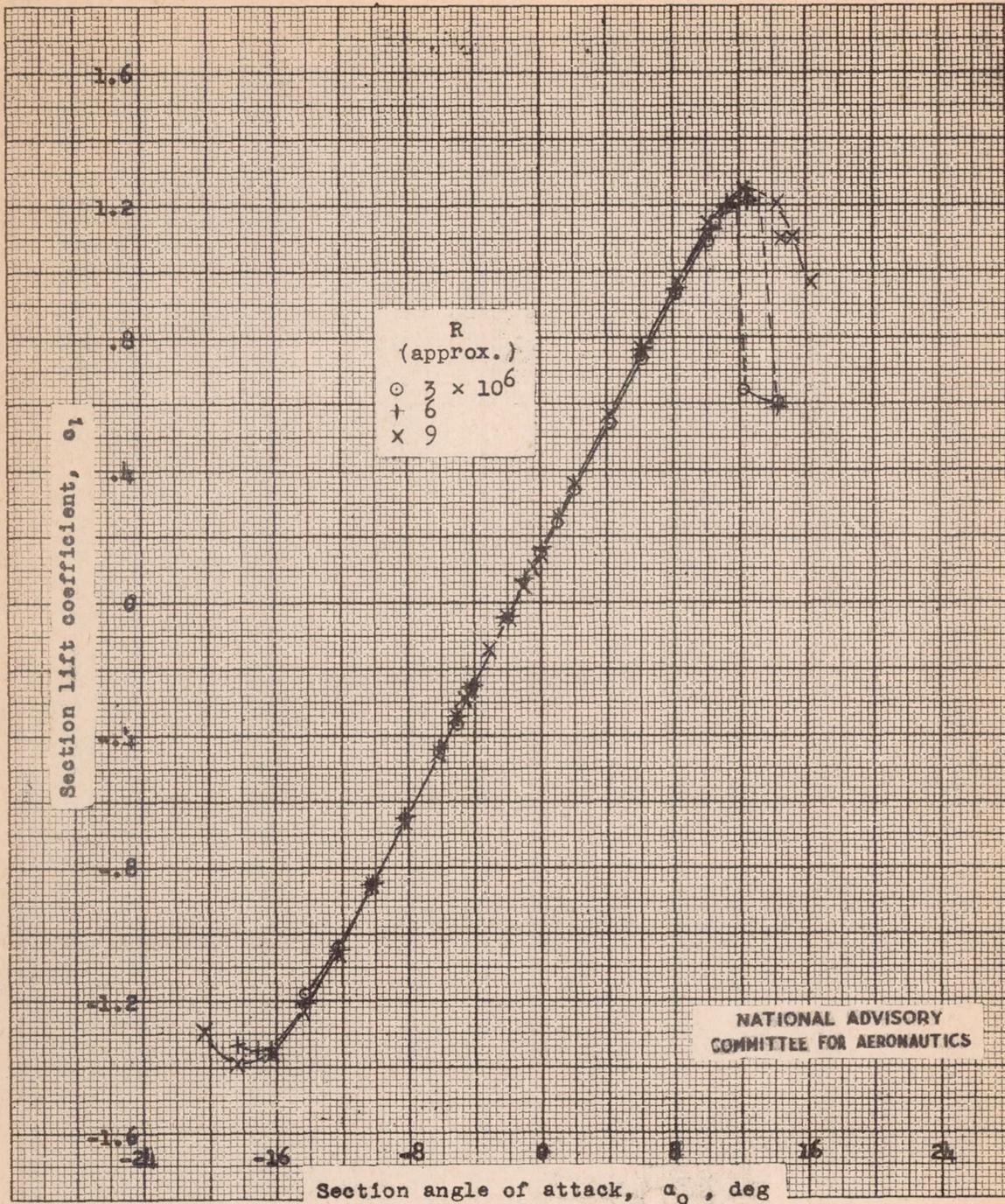
Figure 17.- Lift characteristics of a low-drag horizontal-tail
    section equipped with a 0.35c sealed internally balanced
    elevator. $\delta_e = 0°$; test, TDT 581.

Figure 18.- Hinge-moment characteristics of a 0.35c sealed internally
balanced elevator on a low-drag horizontal-tail section.
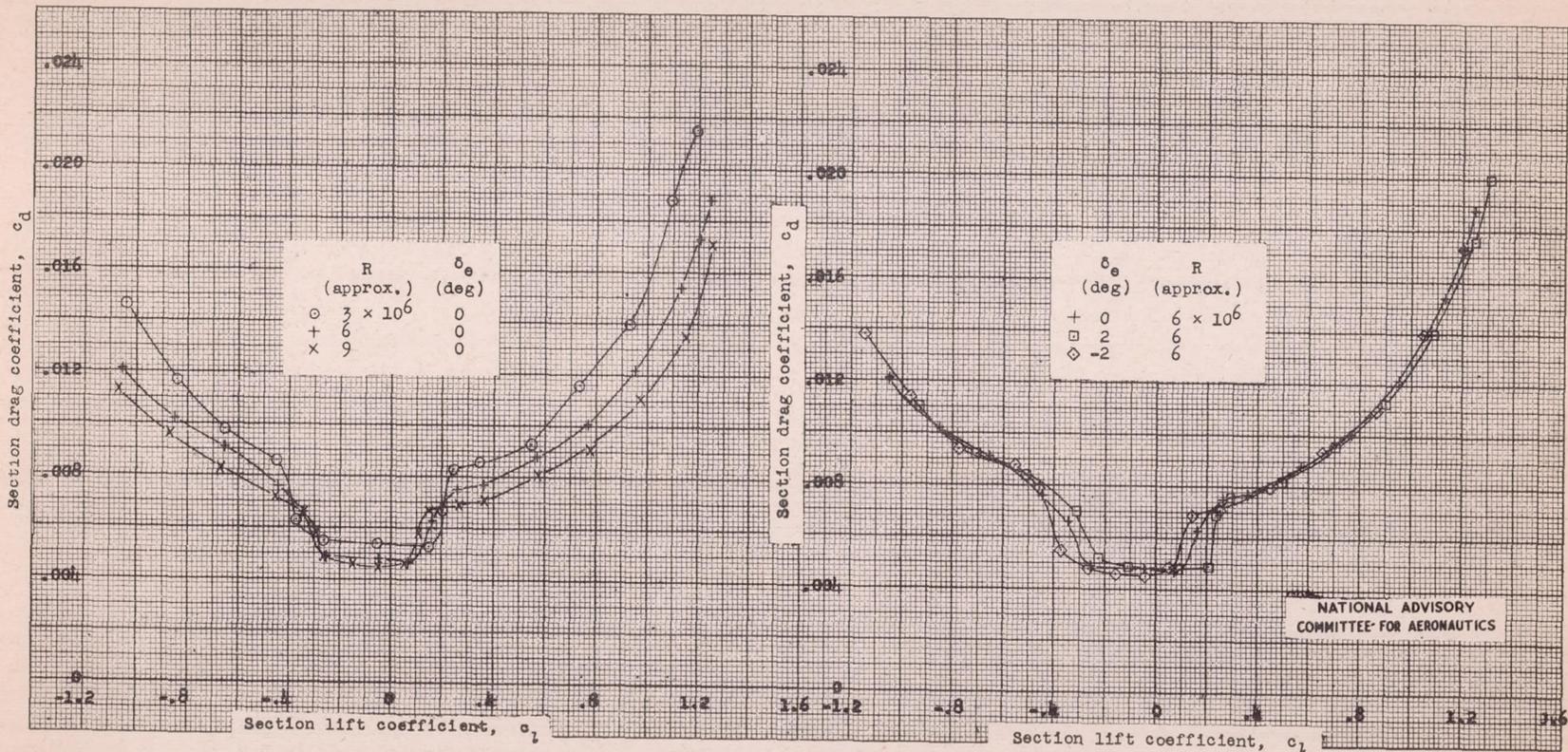R = 6 × 10⁶ (approx.); tests, TDT 581 and 589.

Fig. 19   NACA TN No. 1048
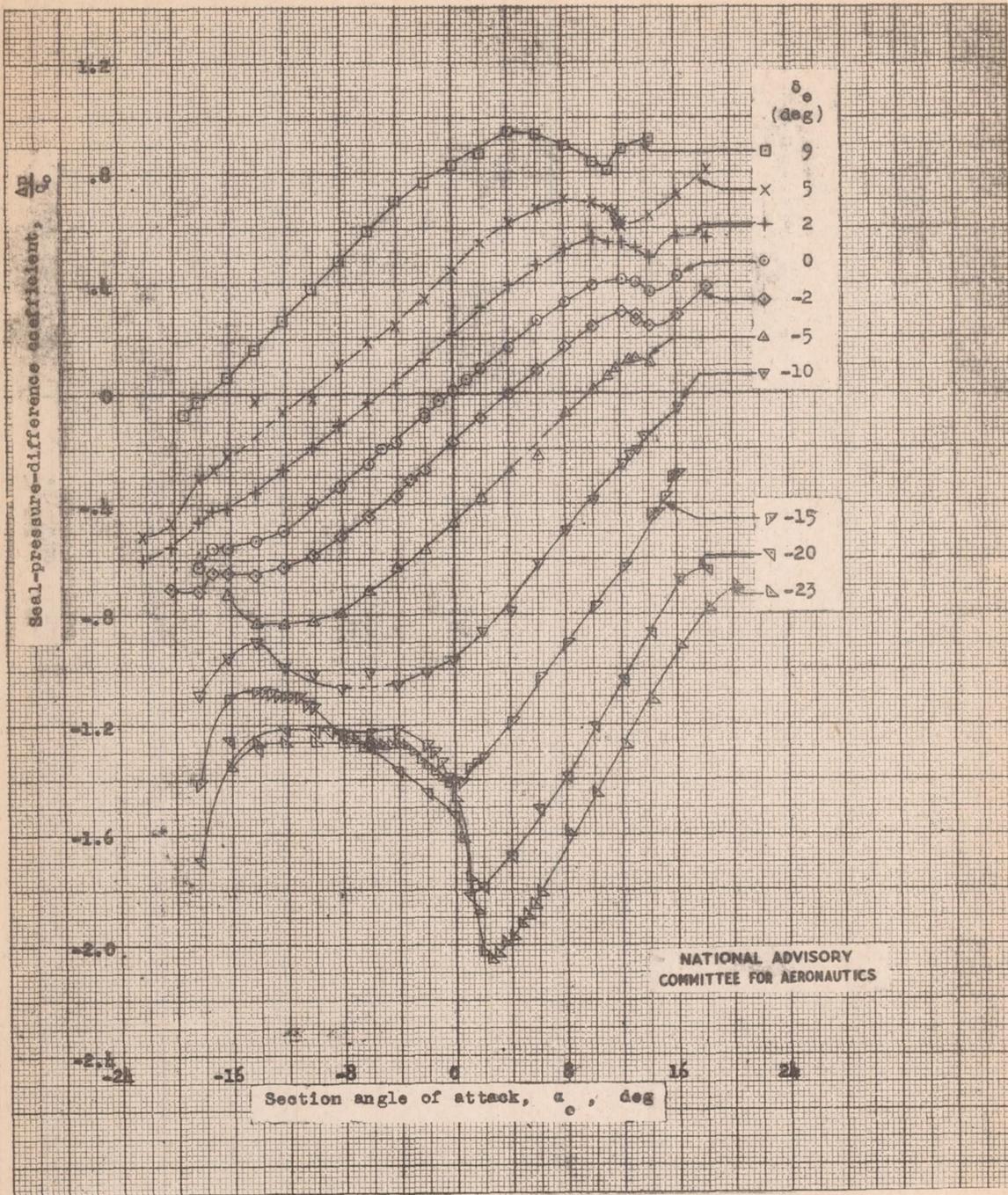
Figure 19.— Variation of $\frac{\Delta p}{q_0}$ with α_0 for a 0.35c sealed internally balanced elevator on a low-drag horizontal-tail section. $R = 6 \times 10^6$ (approx.); tests, TDT 581 and 589

Figure 20.- Drag characteristics of a low-drag horizontal-tail section equipped with a 0.35c sealed internally balanced elevator.   Tests, TDT 581 and 589.

Fig. 20

Fig. 21   NACA TN No. 1048
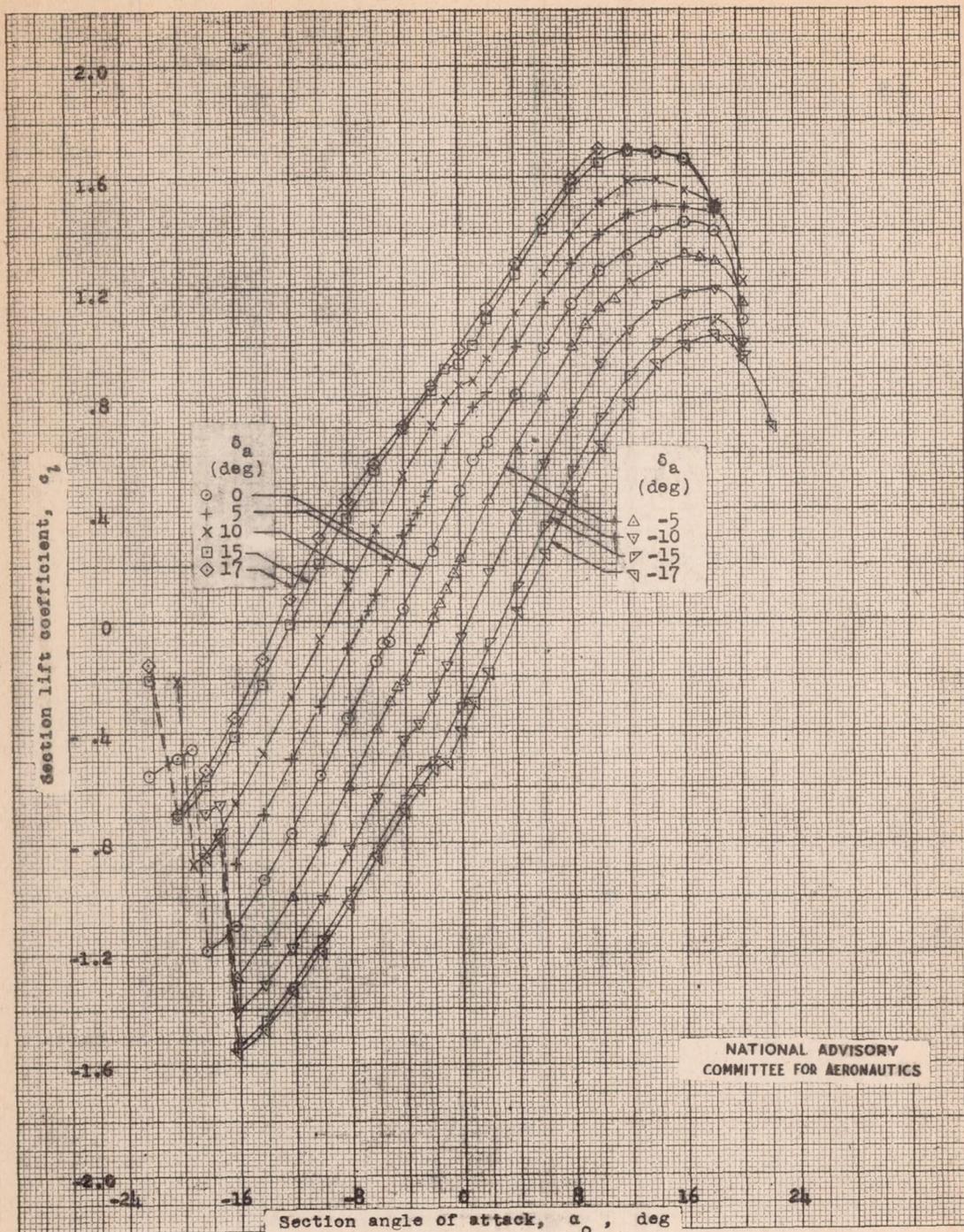
Figure 21.- Lift characteristics of a low-drag wing section equipped with a
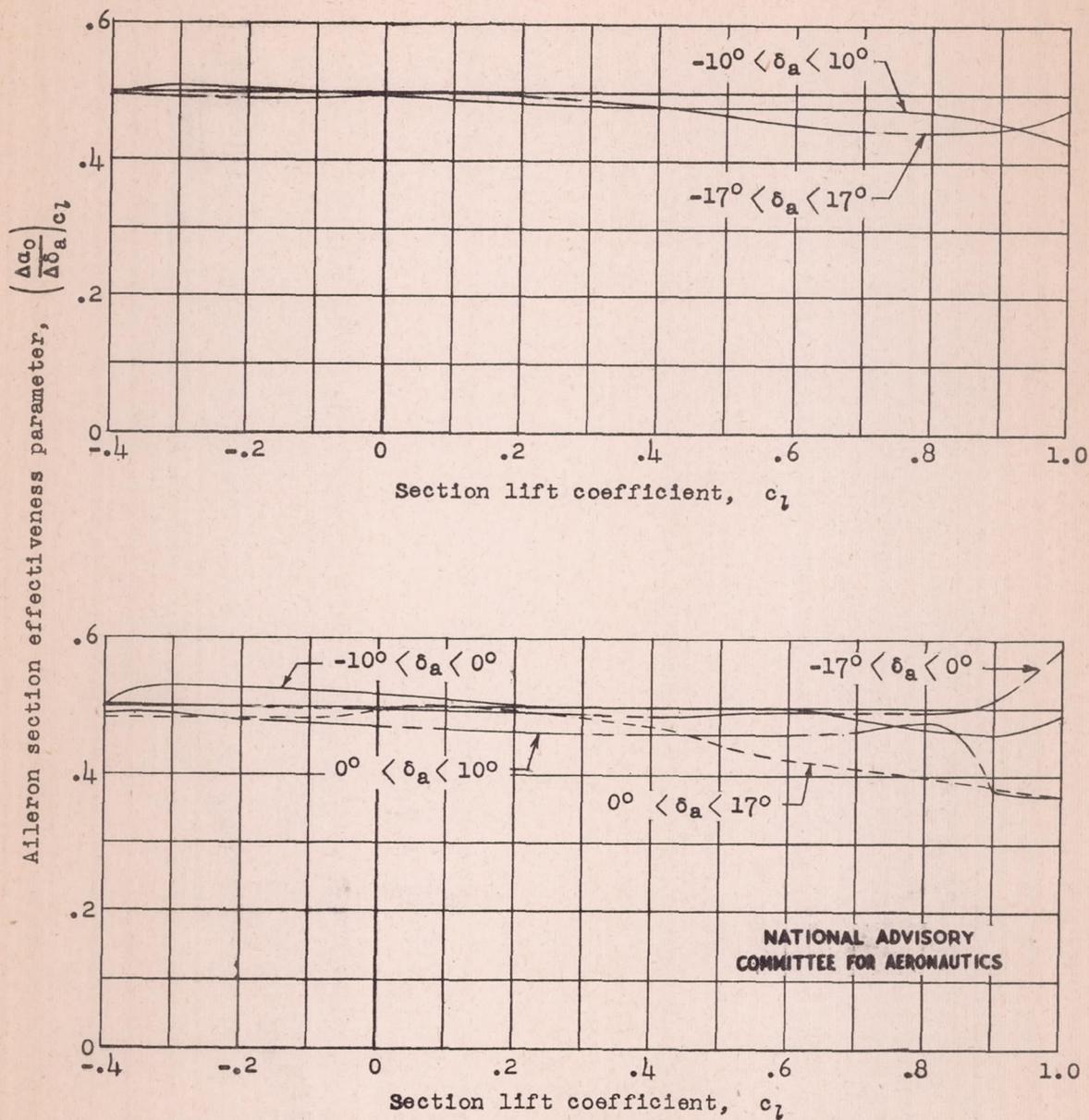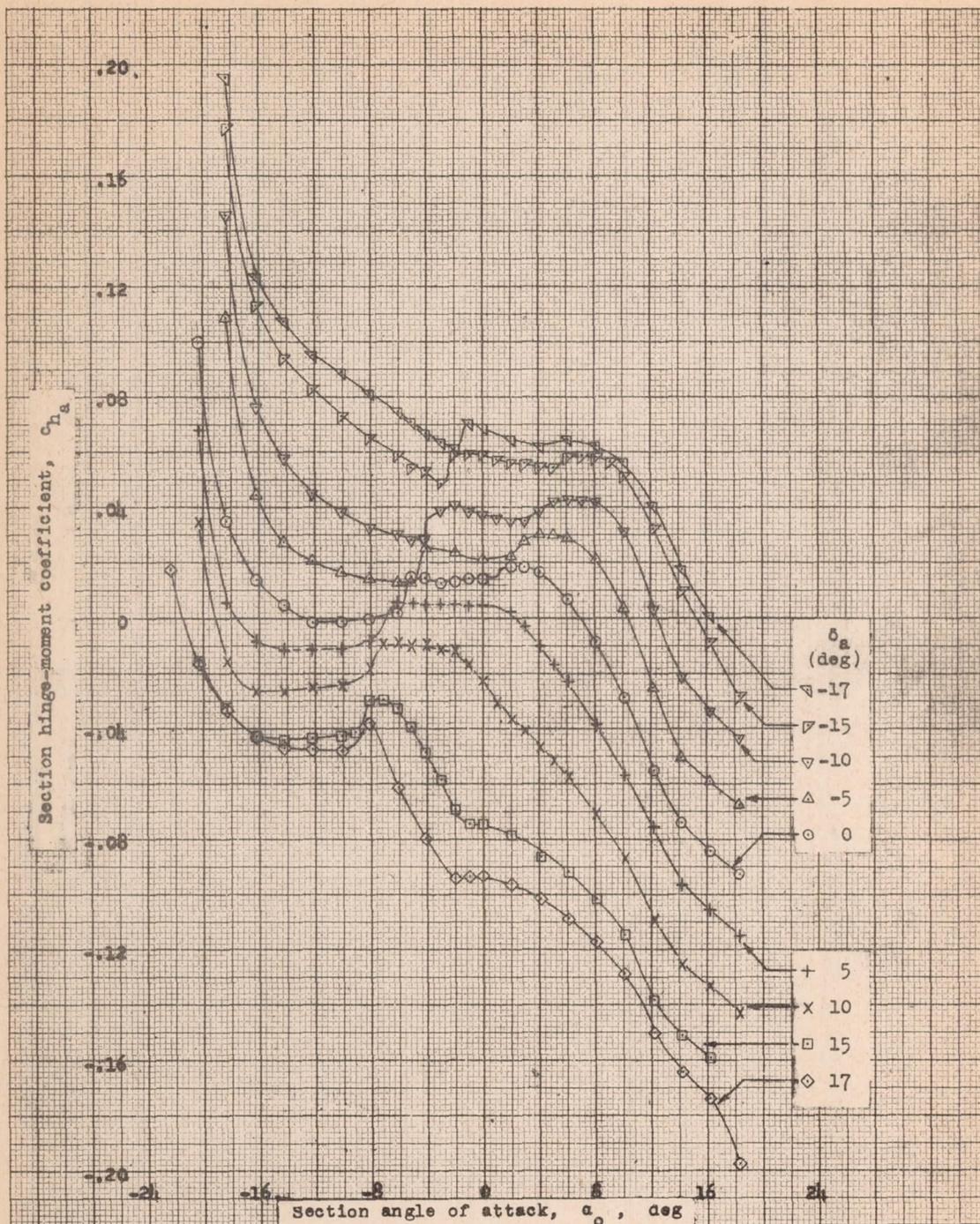0.22c sealed internally balanced aileron.   R = 6 × 10^6 (approx.);
test, TDT 583.

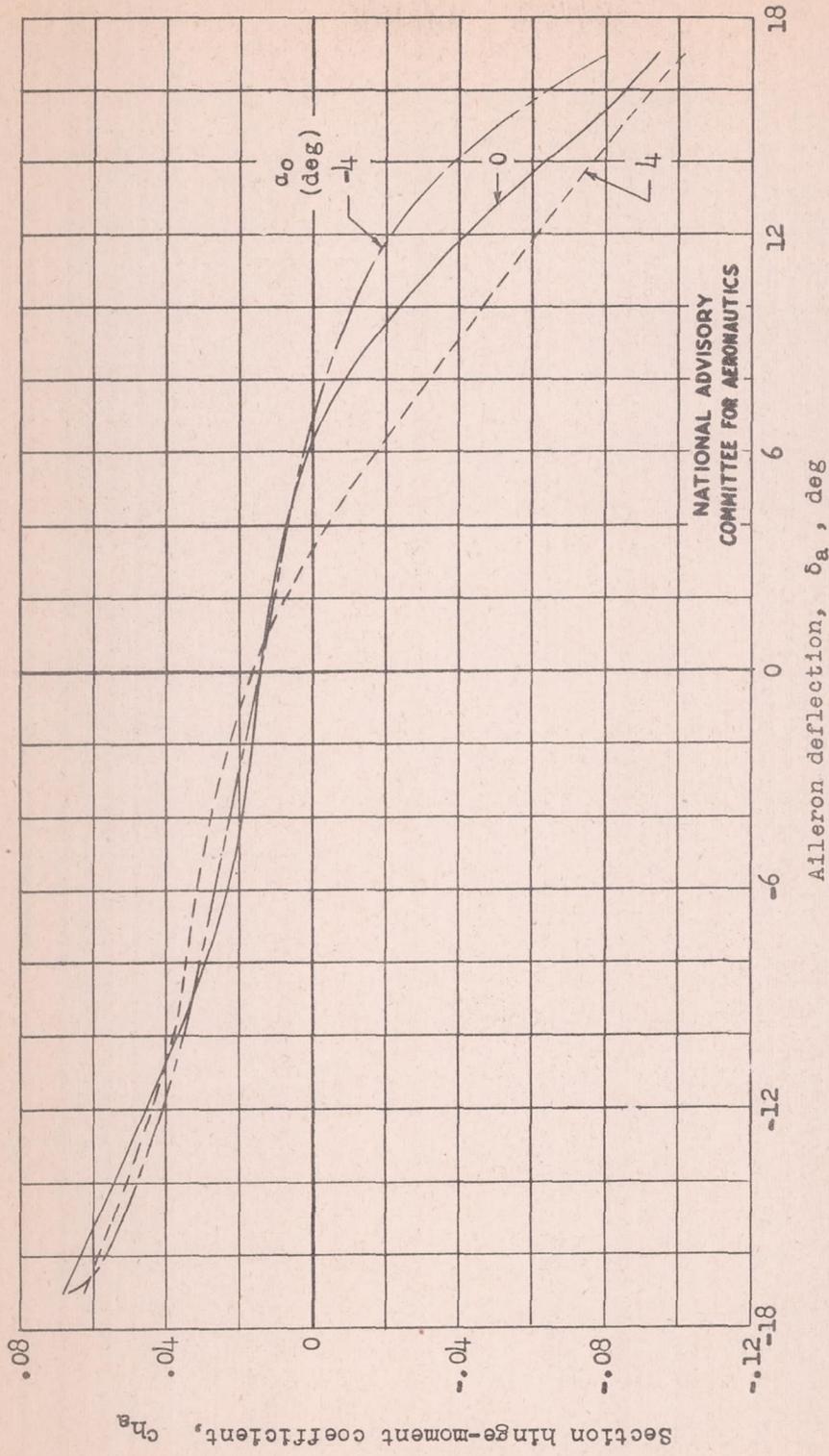Figure 22.- Variation of $\left(\dfrac{\Delta a_0}{\Delta \delta_a}\right)_{c_l}$ with c_l for a low-drag wing section equipped with a 0.22c sealed internally balanced aileron. $R = 6 \times 10^6$ (approx.).

(a) Variation of c_{h_a} with a_o.

NATIONAL ADVISORY
COMMITTEE FOR AERONAUTICS

Figure 23.- Hinge-moment characteristics of a 0.22c sealed
    internally balanced aileron on a low-drag wing section.
    R = 6 × 10⁶ (approx.); test, TDT 583.

Section hinge-moment coefficient, c_{h_a}

Aileron deflection, δ_a, deg

NATIONAL ADVISORY
COMMITTEE FOR AERONAUTICS

(b) Variation of c_{h_a} with δ_a.

Figure 23.- Concluded.

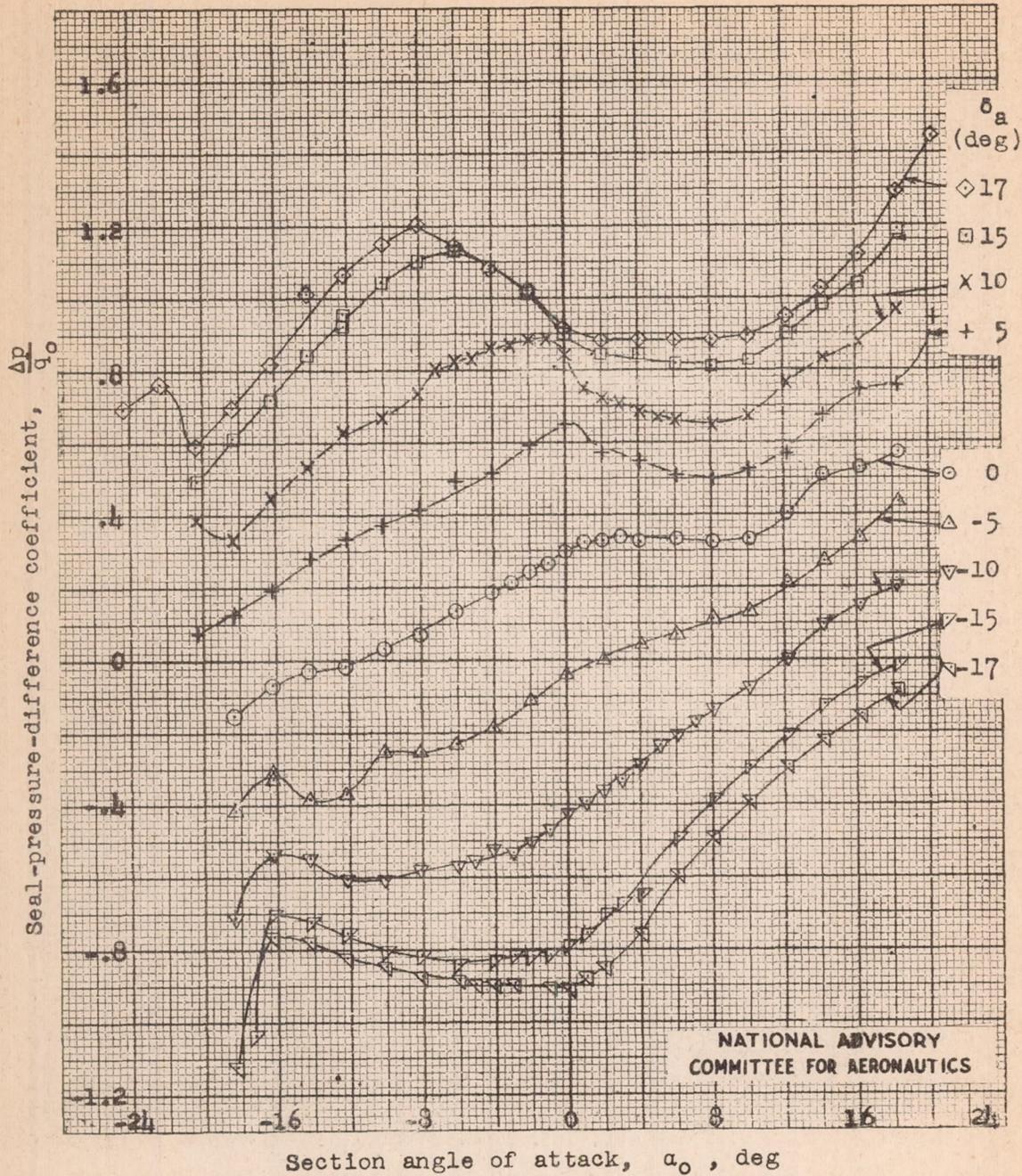Fig. 24   NACA TN No. 1048

Figure 24.- Variation of $\frac{\Delta p}{q_o}$ with α_o for a 0.22c sealed internally balanced aileron on a low-drag wing section. $R = 6 \times 10^6$ (approx.); test, TDT 583.
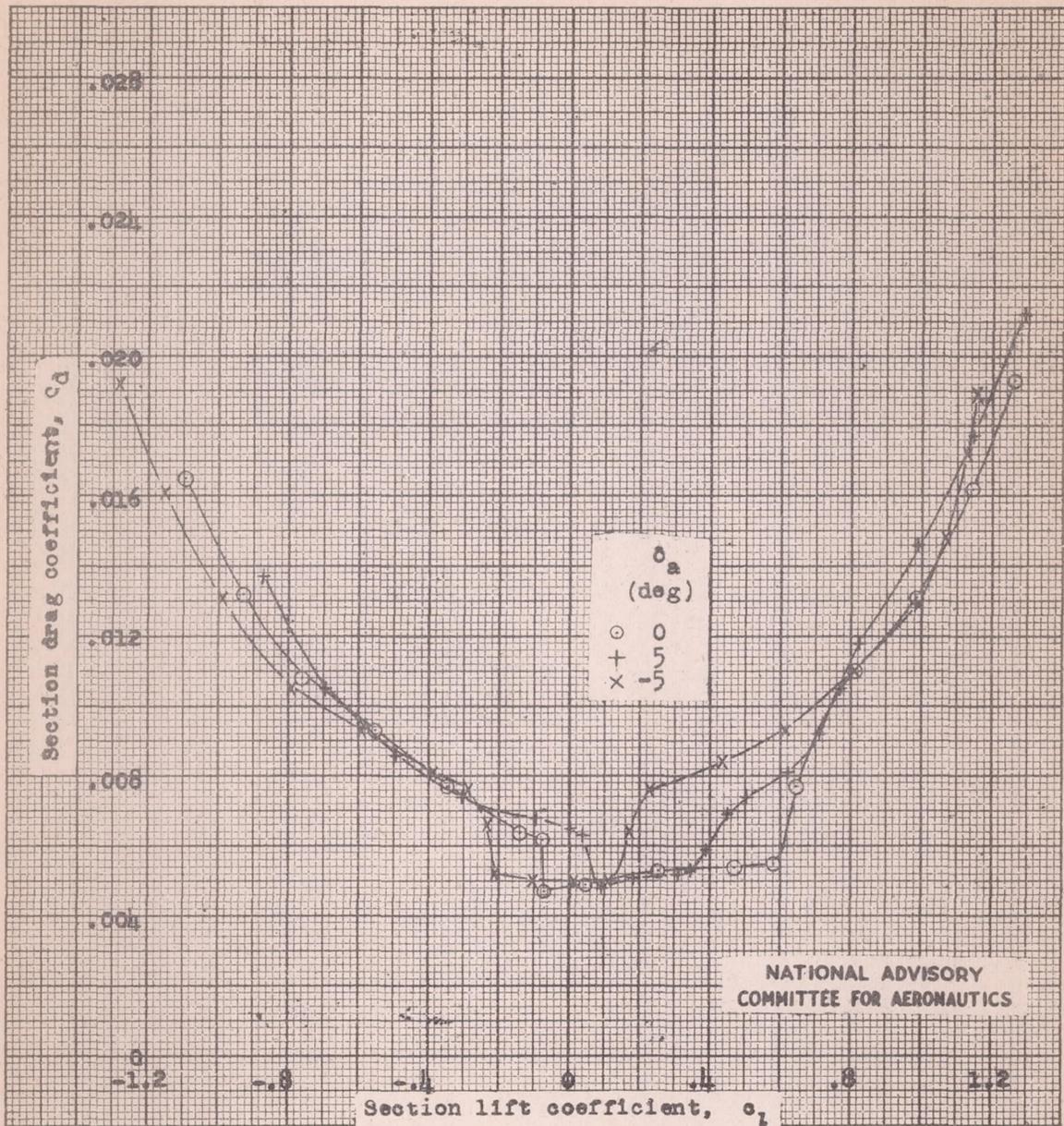
Figure 25.- Drag characteristics of a low-drag wing section
equipped with a 0.22c sealed internally balanced aileron.
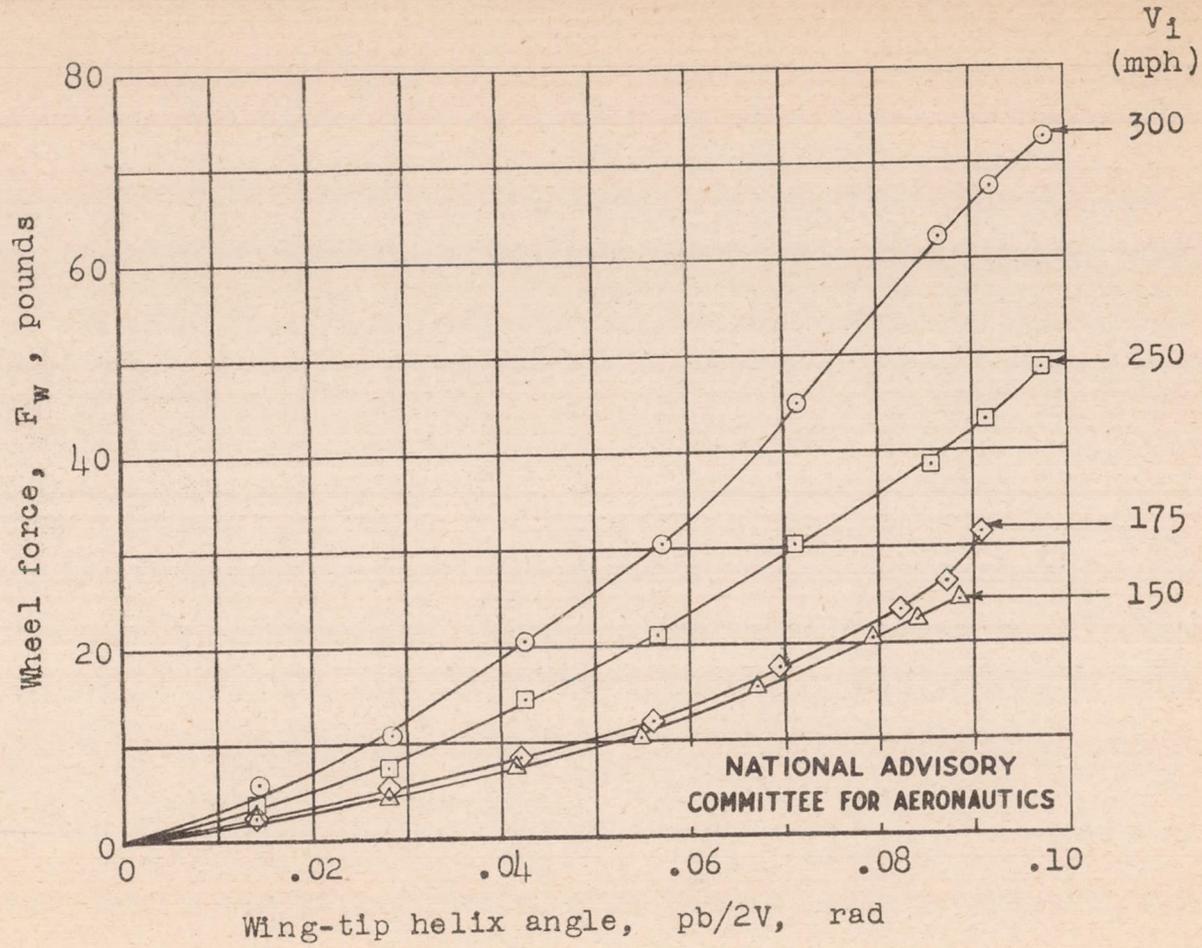$R = 6 \times 10^6$ (approx.); test, TDT 583.

Fig. 26

Figure 26.- Variation of aileron wheel force with wing-tip helix angle.